NOAA OAR Special Report

PMEL Tsunami Forecast Series: Vol. #
A Tsunami Forecast Model for Keauhou, Hawaii

(Draft)

Liujuan Tang

August 2011

NOAA Center for Tsunami Research (NCTR)
Pacific Marine Environmental Laboratory

Contents

List of Tables

PMEL Tsunami Forecast Series: Vol.
A Tsunami Forecast Model for Keauhou, Hawaii

Liujuan Tang

Abstract

This study describes the development, validation, and testing of a tsunami forecast model for Keauhou, Hawaii. Based on the Method of Splitting Tsunamis (MOST) model, the forecast model is capable of simulating four hours of tsunami wave dynamics at a resolution of 1 arc sec (~30 m) in about 14 minutes of computational time. A reference inundation model of higher resolution of 1/3 arc-sec (~10 m) was also developed in parallel to provide modeling references for the forecast model. Both models were tested for seventeen past tsunamis and a set of eighteen simulated magnitude 9.3 tsunamis.

The numerical consistency between the model outputs on the amplitude time series at warning point, maximum amplitude, and current in the forecast area, are good in general. The difference in the maximum amplitude at the warning point between the reference and forecast models is within 17 cm when it is under 1 m (except the 1946 tsunami, which shows a 31 cm difference for a maximum amplitude of 65 cm), and less than 20% when it is greater than 1 m (except the magnitude 9.3 tsunamis from Central Aleutian, Kamchatka and Izu subdection zones, from which the difference can be 33%).

The simulated magnitude 9.3 tsunamis show an impressive local variability of tsunami amplitudes at Keauhou and indicate the complexity of forecasting tsunami amplitudes at a coastal location. It is essential to use high-resolution models in order to provide accuracy that is useful for coastal tsunami forecast for practical guidance.

The study highlights that tsunamis from Japan, Kamchatka, Northern Tonga (Samoa), Isu, Southern Chile, East Philippines, and Central Aleutian subduction zones can potentially generate large amplitude waves in Keauhou. It also shows the water front at Kahaluu Beach Park and at the end of Keauhou bay are under high flooding risk.

1 Background and Objective

The National Oceanic and Atmospheric Administration (NOAA) Center for Tsunami Research at NOAA's Pacific Marine Environmental Laboratory (PMEL) has developed a tsunami forecasting system for operational use by NOAA's two Tsunami Warning Centers located in Hawaii and Alaska (Titov et al., 2005; Titov, 2009). The forecast system combines real-time deep-ocean tsunami measurements from Deep-ocean Assessment and Reporting of Tsunami (DART) buoys (*Gonzalez et al*., 2005; *Bernard et al.*, 2006, *Bernard and Titov*, 2007) with the MOST model, a suite of finite difference

numerical codes based on nonlinear long wave approximation (*Titov and Synolakis*, 1998; *Titov and Gonzalez*, 1997; *Synolakis*, *et al*., 2008) to produce real-time forecasts of tsunami arrival time, heights, periods, and inundation. To achieve accurate and detailed forecast of tsunami impact for specific sites, high-resolution tsunami forecast models are under development for United States coastal communities at risk (Tang *et al.*, 2008[a]; 2009[a]). The resolution of these models has to be high enough to resolve the dynamics of a tsunami inside a particular harbor, including influences of major harbor structures such as breakwaters. These models have been integrated as crucial components into the forecast system.

Presently, a system of 41 DART buoys (32 U.S.-, 1 Russian-,1 Chilean-, and 6 Australian- owned) is monitoring tsunami activity in the Pacific Ocean, as shown in Figure 1. Globally, the network consists of 52 tsunameters deployed in the Atlantic Ocean, the Pacific Ocean, Caribbean, and the Gulf of Mexico. The precomputed propagation models currently have 1,106 scenarios to cover Pacific tsunami sources (1,691 globally), and the high-resolution forecast inundation models are now set up for 43 U.S. coastal communities. The fully implemented system will use real-time data from the DART network to provide high-resolution tsunami forecasts for at least 75 communities in the U.S. by 2013 (Titov, 2009). Since its first testing in the 17 November 2003 Rat Island tsunami, the forecast system has produced experimental realt-ime forecasts for 17 tsunamis in the Pacific and Indian oceans (Titov et al., 2005; Wei et al., 2008; Titov, 2009; Tang et al., 2011). The forecast methodology has also been tested with the data from nine additional events that produced the deep-ocean data.

Two recent tsunamis, the 2009 Samoa and 2011 Japan tsunamis, caused flooding and damaging in the Kahaluu-Keauhou area, highlighting the need of a forecast flooding model for this area. The report describes the development, testing, and applications of the Keauhou forecast model. The objective is to provide NOAA's Tsunami Warning Centers the ability to assess danger posed to Keauhou following tsunami generation in the Pacific Ocean Basin and to provide accurate and timely forecasts to enable the community to respond appropriately. A secondary objective is to explore the potential tsunami impact from earthquakes at major subduction zones in the Pacific using the developed flooding model.

The report is organized as follows: Section 2 briefly introduces NOAA's tsunami forecast methodology, Section 3 describes the model development, and Section 4 presents the results and discussion, which includes sensitivity of the forecast model to model setup, verification, and testing for past and simulated tsunamis. A summary and conclusion are provided in section 5.

2 Forecast Methodology

NOAA's real-time tsunami forecasting scheme is a process comprised of two steps: (1) construction of a tsunami source via inversion of deep ocean DART observations with

pre-computed tsunami source functions; and (2) coastal predictions by running high-resolution forecast models in real time (*Titov et al*., 1999; *Titov et al*., 2005; Tang *et al*., 2009[a]). The DART-constrained tsunami source, the corresponding offshore scenario from the tsunami source function database, and high-resolution forecast models cover the entire evolution of earthquake-generated tsunamis, i.e., generation, propagation, and coastal inundation, providing a complete tsunami forecast capability.

2.1 Construction of A Tsunami Source Based on DART Observations and Tsunami Source Functions

Several real-time data sources, including seismic data, coastal tide gage, and deep-ocean data have been used for tsunami warning and forecast (*Satake et al*., 2008; *Whitmore*, 2003; *Titov,* 2009). NOAA's strategy for the real-time forecasting is to use deep-ocean measurements at DART buoys as the primary data source due to several key features. (1) The buoys provide a direct measure of tsunami waves, unlike seismic data, which are an indirect measure of tsunamis. (2) The deep ocean tsunami measurements are in general the earliest tsunami information available, since tsunamis propagate much faster in deep ocean than in shallow coastal area where coastal tide gages are used for tsunami measurements. (3) Compared to coastal tide gages, DART data with a high signal to noise ratio can be obtained without interference from harbor and local shelf effects. (4) Wave dynamics of tsunami propagation in deep ocean is assumed to be linear (Liu, 2009). This linear process allows application of efficient inversion schemes.

Time series of tsunami observations in deep-ocean can be decomposed into a linear combination of a set of tsunami source functions in the time domain by a linear least squares method. We call coefficients obtained through this inversion process *tsunami source coefficients*. The magnitude computed from the sum of the moment of tsunami source functions multiplied by the corresponding coefficients is referred as the *tsunami moment magnitude* (T_{Mw}), to distinguish from the seismic moment magnitude M_w, which is the magnitude of the associated earthquake source. While the seismic and tsunami sources are in general not the same, this approach provides a link between the seismically-derived earthquake magnitude and the tsunami observation-derived tsunami magnitude.

During real-time tsunami forecast, seismic waves propagate much faster than tsunami waves, so the initial seismic magnitude can be estimated before the DART measurements are available. Since time is of the essence, the initial tsunami forecast is based on the seismic magnitude only. The T_{Mw} will update the forecast when it is available via DART inversion using the tsunami source function database.

Titov et al.(1999; 2001) conducted sensitivity studies on far-field deep-water tsunamis for different parameters of elastic deformation models described in *Gusiakov* (1978) and *Okada* (1985). The results showed source magnitude and location essentially define far-field tsunami signals for a wide range of subduction zone earthquakes. Other parameters have secondary influence and can be pre-defined during a forecast. Based on these results, tsunami source function databases for Pacific, Atlantic, and Indian Oceans have been built using pre-defined source parameters: length = 100 km, width = 50 km, slip = 1 m, rake = 90, and rigidity = 4.5 x 10^{10} N/m^2. Other parameters are location-

specific; details of the databases are described in *Gica et al*. (2008). Each tsunami source function is equivalent to a tsunami from a typical M_w = 7.5 earthquake with defined source parameters. Figure 1 shows the locations of tsunami source functions in the Pacific Ocean.

The database can provide offshore forecast of tsunami amplitudes and all other wave parameters immediately, once the inversion is complete. The tsunami source, which combines real-time tsunami measurements with tsunami source functions, provides an accurate offshore tsunami scenario without additional time-consuming model runs.

2.2 Real-time Coastal Predictions by High-Resolution Forecast Models.

High-resolution forecast models are designed for the final stage of the evolution of tsunami waves: coastal runup and inundation. Once the DART-constrained tsunami source is obtained (as a linear combination of tsunami source functions), the pre-computed time series of offshore wave height and depth-averaged velocity from the model propagation scenario are applied as the dynamic boundary conditions for the forecast models. This saves the simulation time for basin wide tsunami propagation. Tsunami inundation is a highly nonlinear process. Therefore a linear combination would not, in general, provide accurate solutions. A high-resolution model with accurate bathymetric/topographic data is also required to resolve shorter tsunami wavelengths near shore. The forecast models are constructed with the MOST model, a finite difference tsunami inundation model based on nonlinear shallow-water wave equations (*Titov and Gonzalez,* 1997). Each forecast model contains three telescoping computational grids with increasing resolution, covering regional, intermediate, and near-shore areas. Runup and inundation are computed at the coastline. For example, Figure 2 shows the forecast model setup for several tsunami forecast models in Hawaii, detailing the telescoping grids used:

(a) One regional grid of 2-arc-minute (~3600m) resolution covers the main Hawaiian Islands (Figure 2.a).

(b) Then the Hawaiian Islands are divided into four intermediate grids of 12 to 18 arc sec (~ 360 –540m) for four natural geographic areas (Figures 2.b 1-4):

(b1) Ni'ihau, Ka'ula Rock, and Kauai (Kauai complex),

(b2) Oahu,

(b3) Molokai, Maui, Lanai, and Kaho'olawe (the Maui Complex),

(b4) Hawaii.

(c) Each intermediate grid contains 2 arc sec (~60 m) near-shore grids (Figs. 2.c 1-4).

The highest resolution grid includes the population center and tide stations for forecast verification. The grids are derived from the best available bathymetric/topographic data at the time of development, and will be updated as new survey data become available.

The forecast models are optimized for speed and accuracy. By reducing the computational areas and grid resolutions, each model is optimized to provide 4-hour

event forecasting results in minutes of computational time using one single processor, while still providing good accuracy for forecasting. To ensure forecast accuracy at every step of the process, the model outputs are validated with historical tsunami records and compared to numerical results from a reference inundation model with higher resolutions and larger computational domains. In order to provide long duration warning guidance during a tsunami event, each forecast model has been tested to output up to 24-hour simulations after tsunami generation.

3 Model Development

3.1 Forecast area

The main Hawaiian Islands are the younger and southern portion of the Hawaii Archipelago. From northwest to southeast, the islands form four natural geographic groups with shared channels and inter-island shelf, including (1) Ni'ihau, Ka'ula Rock, and Kauai, (Kauai complex) (2) Oahu, (3) Molokai, Maui, Lanai, and Kaho'olawe, (the Maui Complex), and (4) Hawaii. Kahaluu-Keauhou is located at the southwest shore of the Big Island of Hawaii. As of the 2010 Census, it had a resident population of 3549 and 1457 households. Figure 3 presents an aerial photo of this area, and a chart is shown in Figure 4. The population density data is in Figure 5.

The Island of Hawaii (Big Island) is located at the southeast end of the Hawaii Archipelago (Figure 2). To its northwest, there is the Maui complex, with the deep Alenuihaha Channel in between (water depth greater 200m). Gentle slope from 0 to 100 m water depth followed by sudden steep offshore slopes from 100m down to 4000 m depth characterize the coast of Kahaluu-Keauhou area. From 0 to 100m depth, the slope is quite gentle, only 0.013. From 100m to 1000m water depth is the steepest offshore slope of 0.3822, and then 0.15 slope from 1000m to 4000m depth.

No tide station exists in the forecast area. The Kawaihae tide station on the same (west) coast of the Island is approximately 53 km to the north - the closest station to this area. At Kawaihae station, the mean range of tide is 0.461m, and the Mean High Water is 0.222 m above Mean Sea Level. Since no tide gage is in the area, a point (204.03740740°E, 19.5616666 ° N) at 3.6m water depth near the end of Keauhou bay was chosen as the warning point (Figure 7d).

3.2 Tsunami history and data

The Hawaii Islands have a long history of destructive tsunamis (Pararas-Carayannis, 1969; Soloviev and Go, 1984; Lander and Lockridge, 1989) generated by both distant and local sources. The descriptions for Keauhou were extracted from the references as

follows. The height in Pararas-Carayannis (1969) refers to maximum runup height or amplitude. Walker (2004) summarized the runups on the Island of Hawaii for the 1946, 1952, 1957, 1960 and 1964 tsunamis (Figure 5).

The earliest recorded tsunami damage at Keauhou was on April 3, 1868, when a magnitude 7-7.5 earthquake occurred in S.E. Hawaii. “Right after the quake ended, the sea inundated a to the two basaltic columns on the road to Keauhou; all buildings were swept away” (Pararas-Carayannis, 1969).

On June 15, 1896, an earthquake at Sanriku, Japan produced a 9.1 m high tsunami at Keauhou (Pararas-Carayannis, 1969).

On August 9,1901, an earthquake at Rikuchu, Japan created a tsunami which swept a house away at Keauhou. Kailua was flooded. No disturbance was noticed elsewhere in the Hawaiian Islands (Pararas-Carayannis, 1969).

On April 1, 1946, a 4 m high tsunami was observed for the Unimak earthquake (Pararas-Carayannis, 1969).

On March 17, 1952, an earthquake at Hokkaido, Japan produced a 0.9 m high tsunami at Keauhou (Pararas-Carayannis, 1969).

On March 9, 1957, a 2.1m high tsunami was observed at Keauhou for the Andreanof Island earthquake (Pararas-Carayannis, 1969).

On May 22, 1960, a 3.7 m high tsunami was observed at Keauhou for the Chile earthquake (Pararas-Carayannis, 1969).

On September 29, 2009, the Samoa tsunami flooded the Parking area near the Keauhou Boat Ramp.

On March 11 2011, the Japan tsunami hit Keauhou bay hard. Water slammed into the end of the Keauhou bay, destroying Keauhou Yacht Club and severely damaging three ocean sports activity offices (Bracken, 2011). “Well into the day on Friday, surges continued to sweep over the road, invade nearby structures and throw fish far back up onto land” (Rizzuto, 2011). The Keauhou Boat Ramp and Keauhou Pier were also damaged. The Kahalulu Beach Park was flooded, with rocks and debris left everywhere. The water also undermined a small pavilion when waves crashed over the top (Bracken, 2011).

As an area that has repeatedly been damaged and flooded by tsunamis, Keauhou is in need of a forecast model to aid site-specific evacuation decisions.

3.3 Bathymetry and Topography

Tsunami inundation modeling requires accurate bathymetry in coastal area as well as high resolution topography and bathymetry in the near-shore area. Two gridded digital elevation models (DEMs), one at medium resolution (6 arc sec) for Hawaiian Islands and a high resolution (1/3 arc sec) DEM for Keauhou, were developed.

3.3.1 Hawaiian DEM in 6-arc-sec resolution

The 6" Hawaiian DEM was developed at NOAA center for tsunami research in 2007. The same grid has been used for the forecast model developments for Hilo, Kahului, Honolulu, Pearl Harbor, and Lahaina (Tang et al, 2009; 2010). The grid was compiled from several data sources; Figure 7a is an overview of the spatial extents of each data source used. In areas where multiple datasets overlapped, higher-resolution and newer datasets were generally preferred, and superseded datasets were used for comparison and verification. An overview of the data sources used was, in general, the data sources listed first superseded data sources listed later when they overlapped.

Source details for the datasets incorporated into the model grids:

- Joint Airborne Lidar Bathymetry Technical Center of Expertise (JALBTCX), US Army Corps of Engineers, Mobile District. Online reference: http://shoals.sam.usace.army.mil/hawaii/pages/Hawaii_Data.htm.
- Monterey Bay Aquarium Research Institute (MBARI) Hawaii Multibeam Survey, Version 1. Online reference: http://www.mbari.org/data/mapping/hawaii/.
- USGS Pacific Seafloor Mapping Project. Online reference: http://walrus.wr.usgs.gov/pacmaps/data.html.
- Japan Agency for Marine-Earth Science and Technology (JAMSTEC) 1998-1999 multibeam bathymetric surveys. Published in: Takahashi, E., *et al*., eds. (2002): *Hawaiian Volcanoes: Deep Underwater Perspectives*. American Geophysical Union Monograph 128.
  JAMSTEC trackline data was recorded by the R/V *Mirai* during transits near in 1999 and 2002. Online reference: http://www.jamstec.go.jp/mirai/index_eng.html.
- United States Army Corps of Engineers (USACE), Honolulu District. Online reference: http://www.poh.usace.army.mil/.
- NOAA National Geophysical Data Center (NGDC). Online reference: http://www.ngdc.noaa.gov/mgg/gdas/gd_sys.html.
- NOAA National Ocean Service (NOS). Sounding points were digitized from NOS nautical charts 19347, 19358, 19359, 19364, 19366, 19342, 19381, and 19324. Sounding data from electronic chart (ENC) 19357 was used. This data was included in relatively shallow regions where other data sources were sparse or unavailable, or for quality control of other sources.
- Smith, W. H. F., and D. T. Sandwell, Global seafloor topography from satellite altimetry and ship depth soundings, *Science*, v. 277, p. 1957-1962, 26 Sept., 1997. Online reference: http://topex.ucsd.edu/WWW_html/mar_topo.html.
- USGS Geological Long-Range Inclined Asdic (GLORIA) surveys. Online data reference: http://walrus.wr.usgs.gov/infobank/

- NOAA Coastal Services Center. http://www.csc.noaa.gov/. The IfSAR topographic data was collected and processed for CSC by Intermap Technologies Inc. The data is subject to a restrictive license agreement and is not publicly available.
- USGS National Elevation Dataset. Online reference: http://seamless.usgs.gov/

The SHOALS LIDAR project, which provides high-resolution unified topographic and bathymetric data for near-shore areas of several Hawaiian Islands, including all of Maui, was essential to accurate modeling of reef and intertidal regions where conventional bathymetric survey data is usually coarse or unavailable. Quality data in this region is especially essential because bathymetric inaccuracies have great impact on tsunami wave dynamics in shallow water. The 2005 NOAA CSC IfSAR survey of Maui provided similarly valuable high-resolution topography for the entire island, enabling greater confidence in predicting inundation extents. The USGS National Elevation Dataset (NED) was used on other islands outside of the primary study area.

High-resolution gridded datasets derived from multibeam surveys are available for many parts of the archipelago and were used wherever available. In deep water where high-resolution multibeam data were not available, the grid was developed by interpolation of a combination of USGS GLORIA surveys and the Smith and Sandwell two-minute global seafloor dataset.

All selected input datasets were converted to the mean high water (MHW) vertical datum, as necessary. Bathymetry datasets were converted from the survey tidal datum (usually MLLW or MSL) using offset surfaces interpolated from NOS tide gauges at Kahului, Kawaihae (Hawaii), and Kaunakakai (Molokai). The CSC IfSAR topographic data as obtained was vertically referenced to the GRS80 ellipsoid. It was converted to MHW using an offset surface interpolated from seven National Geodetic Survey (NGS) benchmark stations on Maui that had ellipsoid and tidal heights recorded.

Raw data sources were imported to ESRI ArcGIS-compatible file formats. Horizontal positions were reprojected, where necessary, to the WGS84 horizontal geodetic datum using ArcGIS. In the point datasets, single sounding points that differed substantially from neighboring data were removed. Gridded datasets were checked for extreme values by examination of contour lines and, where available, by comparison between multiple data sources.

To compile the multiple data sources into a single grid, subsets of the source data were created in the priority order described above. A triangulated irregular network (TIN) was created from the detided vector point data (geodas, usace, csc_lidar). Also added to the TIN were points taken from the edges of the gridded data regions to ensure a smooth interpolated transition between areas with different data sources. This TIN was linearly interpolated using ArcGIS 3D Analyst to produce intermediate 1 arc sec and 6 arc sec raster grid. The gridded datasets were then bilinearly resampled to these resolutions and overlaid on top of the intermediate grids.

3.3.2 Keauhou DEM in 1/3-arc-sec resolution

A high-resolution DEM in 1/3-arc-sec (~10m) was developed for the Keauhou area by the National Geophysical Data Center (Carignan et al., 2011). The DEM was generated from diverse digital datasets in the region (grid boundary and sources shown in Figure 7b). The topographical Lidar data from State of Hawaii Civil Defencse /FEMA and HI DBEDT (Department of Business, Economic Development & Tourism) have approximately 1 m special resolution. The detail of the data sources and methodology used in developing the Keauhou DEM can be found in (Carignan et al., 2011).

The bathymetry and topography used in the development of this forecast model were based on the digital elevation model provided by the National Geophysical Data Center, and the author considers it to be a good representation of the local topography/bathymetry. As new digital elevation models become available, forecast models will be updated and report updates will be posted at http://nctr.pmel.noaa.gov/forecast_reports/.

3.4 Model Setup

By sub-sampling from the DEMs described in Section 3.3, two sets of computational grids were derived for Keauhou, a reference inundation model (Figure 8) and the optimized forecast model (Figure9). The reference grids consist of three levels of telescoped grids with increasing resolution. The regional grid covers the major Hawaiian Islands (Fig. 8a), and the coastal grids cover the Island of Hawaii (Figure 8b). Run-up and inundation simulations are computed on the coastline (Fig. 8c). The optimized forecast model has three levels of telescoped grids (Fig ure 9). Grid details at each level and input parameters are summarized in Table 3.

4 Results and Discussion

4.1 Verification and Testing of the Forecast Model

Since no tide gage data was available at Keauhou, we evaluate the forecast model performance through comparison of tsunami amplitude time series, maximum amplitude, and current at the forecast area to the results from the reference model

Both the reference and the forecast models for Keauhou were tested with the seventeen past tsunamis summarized in Table 2. Figures 10 shows the comparisons of modeled amplitude time series at the warning point computed by the reference and forecast models. The computed maximum water elevation above MHW and maximum current of the seventeen tsunamis are plotted in Figure 11. The 2011 Japan tsunami generated the largest amplitude at the warning point (1 m) as well as in the forecast area.

Recorded historical tsunamis provide only a limited number of events, from limited locations. More comprehensive test cases of destructive tsunamis with different directionalities are needed to check the stability and robustness for the forecast model. The same set of eighteen simulated magnitude 9.3 tsunamis as in Tang *et al*. (2008[a], 2009[b]) was selected here for further examination (Table 4). Results computed by the forecast model are compared with those from the high-resolution reference model in Table 4, Figures 12 and 13. Both models were numerically stable for all of the scenarios. Waveforms computed by the forecast model agree well with those from the reference model (Figure 12). Both models compute similar maximum water elevation and inundation in the study area (Figure 13). These results indicate the forecast model is capable of providing robust and stable predictions of long duration for Pacific-wide tsunamis.

The No. 1 Japan, No. 2 Kamchatka, No. 10 Southern Chile, and No. 12 Northern Tonga scenarios produced inundation at Keauhou. The computed maximum wave amplitude reaches 3.6 m at the warning point of the Japan scenario. Tsunami waves in the study area vary significantly for the eighteen magnitude 9.3 scenarios. These results show the complexity and high nonlinearity of tsunami waves near shore, which again demonstrate the value of the forecast model for providing accurate site-specific forecast details.

4.2 Uncertainty of the forecast results

Figure 14 shows the difference of the maximum wave amplitude at the warning point between the forecast and reference models for the 35 scenarios, which includes the 17 past tsunamis and 18 simulated M_w 9.3 scenarios. In general, the forecast model shows smaller maximum amplitudes than those from the reference model. The difference of the maximum amplitude at the warning point between the reference and forecast models is within 17 cm when it is under 1 m (except the 1946 tsunami, which shows a 31 cm difference for a maximum amplitude of 65 cm), and less than 20% when it is greater than 1 m (except the magnitude 9.3 tsunamis from Central Aleutian, Kamchatka, and Izu subdection zones, from which the difference can be 33%).

5 Summary and Conclusions

A tsunami forecast model was developed for the coastal community of Keauhou, Hawaii. The computational grids for the Keauhou forecast model were derived from the best available bathymetric and topographic data sources. The forecast model is optimally constructed at a resolution of 1 arc sec (~30 m) to enable a 4 hr inundation simulation in minutes of computational time. A reference inundation model of higher resolution of 1/3 arc sec (~10 m) was also developed in parallel to provide modeling references for the

forecast model. Both models were tested for seventeen past tsunamis and a set of eighteen simulated magnitude 9.3 tsunamis.

The optimized forecast model can provide a 4-hour site-specified forecast of first wave arrival, amplitudes, and reasonable inundation limit in minutes after receiving tsunami source information constrained by deep-ocean DART measurements.

A tsunami could strike Keauhou with large waves from earthquakes on the Japan, Kamchatka, Northern Tonga, and Southern Chile subduction zones. Attention also needs to be paid to locations from which the main offshore wave energy propagates towards Hawaiian Islands, including the Alaska-Aleutian, Canada, Cascadia, South America, and Vanuatu subduction zones. The water front at Kahaluu Beach Park and area at end of Keauhou bay are under high flooding risk once inundation occurs in the forecast area.

Acknowledgements

The author thanks Elena Tolkova and Jean Newman for assistance; Sandra Bigley for comments, discussion, and editing; and Burak Uslu for providing tables and graphics for the propagation database. Collaborative contributions of the National Weather Service, the National Geophysical Data Center, and the National Data Buoy Center were invaluable.

Funding for this publication and all work leading to development of a tsunami forecast model for Keauhou, Hawaii, was provided by the National Oceanic and Atmospheric Administration. This publication was partially funded by the Joint Institute for the Study of the Atmosphere and Ocean (JISAO) under NOAA Cooperative Agreement No. NA17RJ1232, JISAO Contribution No. xxxx. This is PMEL Contribution No. xxxx.

References

Bernard, E.N., H.O. Mofjeld, V.V. Titov, C.E. Synolakis, and F.I. González (2006): Tsunami: Scientific frontiers, mitigation, forecasting, and policy implications. Proc. Roy. Soc. Lon. A, 364(1845), doi: 10.1098/rsta.2006.1809, 1989–2007.

Bernard, E., and V.V. Titov (2007), Improving tsunami forecast skill using deep ocean observations, Mar. Technol. Soc. J., 40(3), 23–26.

Bracken, S. (2011): Tsunami Cleanup Update. Big Island News Center, March 19, 2011, http://www.bigislandnewscenter.com/tsunami-cleanup-update/.

Carignan, K.S., L.A. Taylor, B.W. Eakins, D.Z. Friday, P.R. Grothe, E. Lim and M. Love (2011): Digital Elevation Models of Keauhou and Kawaihae, Hawaii: Procedures, Data Sources and Analysis. NOAA National Geophysical Data Center (NGDC).

Gica E., Spillane, M.C., Titov, V.V., Chamberlin, C.D. and Newman, J.C. (2008), Development of the forecast propagation database for NOAA's Short-Term Inundation Forecast for Tsunamis (SIFT), NOAA Tech. Memo. OAR PMEL-139, 89pp.

Gusiakov, V.K. (1978): Static displacement on the surface of an elastic space. Ill-posed problems of mathematical physics and interpretation of geophysical data, Novosibirsk, VC SOAN SSSR, 23–51 (in Russian).

Gonzalez, F.I., E.N. Bernard, C. Meinig, M. Eble, H.O. Mofjeld, and S. Stalin (2005): The NTHMP tsunameter network. *Nat. Hazards*, 35(1), Special Issue, U.S. National Tsunami Hazard Mitigation Program, 25-39.

Kanamori, H. and J.J. Ciper (1974): Focal process of the great Chilean earthquake, May 22, 1960. *Physics of the Earth and Planetary Interiors*, 9, 128-136.

Lander, J. F. and P.A. Lockridge (1989): *United States Tsunamis 1690-1988*. NOAA National Environmental Satellite, Data and Information Service, National Geophysical Data Center, Boulder, Colorado, August 1989, 265pp.

Liu, P. L.-F. (2009), Tsunami modeling—Propagation, in The Sea, vol. 15, edited by E. Bernard and A. Robinson, chap. 9, pp. 295– 319, Harvard Univ. Press, Cambridge, Mass.

López, A.M. and E.A. Okal (2006), A seismological reassessment of the source of the 1946 Aleutian 'tsunami' earthquake, *Geophysical Journal International*, Volume 165, Issue 3, Page 835-849, Jun 2006, doi: 10.1111/j.1365-246X.2006.02899.x

National Geophysical Data Center, Global Tsunami Database (2000 BC to present):

http://www.ngdc.noaa.gov/seg/hazard/tsu_db.shtml

Okada, Y., 1985, Surface deformation due to shear and tensile faults in a half-space. *Bull. Seismol. Soc. Am*., 75, 1135-1154.

Rizzuto, J. (2011): Tsunami Hits Keauhou Bay Hard, Big Island News Center, March 13, 2011, http://www.bigislandnewscenter.com/tsunami-hits-keauhou-bay-hard/.

Satake, K., Y. Hasegawa, Y. Nishimae and Y. Igarashi (2008), Recent Tsunamis That Affected the Japanese Coasts and Evaluation of JMA's Tsunami Warnings. OS42B-03, AGU Fall Meeting, San Francisco.

Smith, W. H. F., and D. T. Sandwell (1997), Global seafloor topography from satellite altimetry and ship depth soundings, Science, 277, 1957– 1962.

Soloviev, S.L. and Ch.N Go (1984): *Catalog of Tsunamis on the Eastern Shore of Pacific Ocean*. Canadian Translation of Fisheries and Aquatic Sciences, No. 5078, 293 pp.

Synolakis, C.E., E.N. Bernard, V.V. Titov, U. Kânoğlu, and F.I. González (2008): Validation and verification of tsunami numerical models. *Pure Appl. Geophys*., 165(11–12), 2197–2228.

Tang, L., C. Chamberlin, E. Tolkova, M. Spillane, V.V. Titov, E.N. Bernard, and H.O. Mofjeld (2006): Assessment of potential tsunami impact for Pearl Harbor, Hawaii. NOAA Tech. Memo. OAR PMEL-131.

Tang, L., C. Chamberlin and V.V. Titov, (2008a), Developing tsunami forecast inundation models for Hawaii: procedures and testing, *NOAA Tech. Memo., OAR PMEL -141*, 46 pp.

Tang, L., V.V. Titov, Y. Wei, H.O. Mofjeld, M. Spillane, D. Arcas, E.N. Bernard, C. Chamberlin, E. Gica, and J. Newman (2008b): Tsunami forecast analysis for the May 2006 Tonga tsunami. J. Geophys. Res., 113, C12015, doi: 10.1029/2008JC004922.

Tang, L., V. V. Titov, and C. D. Chamberlin (2009a), Development, Testing, and Applications of Site-specific Tsunami Inundation Models for Real-time Forecasting, *J. Geophys. Res*., doi:10.1029/2009JC005476, in press.

Tang, L., V.V. Titov and C.D. Chamberlin (2009b), A Tsunami Forecast Model for Hilo, Hawaii, NOAA OAR Special Report, PMEL Tsunami Forecast Series: Vol. 1, 44 pp.

Tang, L., V. V. Titov, E. Bernard, Y. Wei, C. Chamberlin, J. C. Newman, H. Mofjeld, D. Arcas, M. Eble, C. Moore, B. Uslu, C. Pells, M. C. Spillane, L. M. Wright, and E. Gica (2012): Direct energy estimation of the 2011 Japan tsunami using deep-ocean pressure measurements. *J. Geophys. Res., 117*, C08008, doi:10.1029/2011JC007635.

Tang, L., C.D. Chamberlin and V.V. Titov (2013): A Tsunami Forecast Model for Kahului, Hawaii. NOAA OAR Special Report, PMEL Tsunami Forecast Series: Vol. 7, (in print).

Titov, V.V. (2009), Tsunami forecasting. Chapter 12 in *The Sea*, Volume 15: Tsunamis, Harvard University Press, Cambridge, MA and London, England, 371–400.

Titov, V.V., F.I. González, E.N. Bernard, M.C. Eble, H.O. Mofjeld, J.C. Newman, and A.J. Venturato (2005): Real-time tsunami forecasting: Challenges and solutions. *Natural Hazards*, 35(1), Special Issue, U.S. National Tsunami Hazard Mitigation Program, 41–58.

Titov, V. V., Mofjeld, H. O., Gonza´ lez, F. I., and Newman, J. C.: 2001, Offshore forecasting of Alaskan tsunamis in Hawaii. In: G. T. Hebenstreit (ed.), Tsunami Research at the End of a Critical Decade. Birmingham, England, Kluwer Acad. Pub., Netherlands, pp. 75–90.

Titov, V.V., H.O. Mofjeld, F.I. Gonzalez and J.C. Newman (1999): Offshore forecasting of Alaska-Aleutian subduction zone tsunamis in Hawaii. NOAA Technical Memorandum. ERL PMEL-114, January 1999, 22 pp.

Titov, V.V. and C.S. Synolakis (1998): Numerical modeling of tidal wave runup. *Journal of Waterway, Port, Coastal and Ocean Engineering*, ASCE, 124(4), 157-171.

Titov, V.V. and F.I. Gonzalez (1997): Implementation and testing of the Method of Splitting Tsunami (MOST) model. NOAA Technical Memorandum. NOAA Pacific Marine Environmental Laboratory, ERL PMEL-112, Nov. 1997, 11 pp.

Pararas-Carayannis, G.(1969): *Catalog of Tsunamis in The Hawaii Islands*, World Data Center A Tsunami, ESSA – Coast and Geodetic Survey, 94 pp.

Walker, D.A. (2004): Regional Tsunami evacuations for the state of Hawaii: a feasibility study on historical runup data. Science of Tsunami Hazards, 22(1), 3-22.

Wei, Y., E. Bernard, L. Tang, R. Weiss, V. Titov, C. Moore, M. Spillane, M. Hopkins, and U. Kânoğlu (2008): Real-time experimental forecast of the Peruvian tsunami of August 2007 for U.S. coastlines. *Geophys. Res. Lett*., 35, L04609, doi: 10.1029/2007GL032250.

Whitmore, P.M. (2003), Tsunami amplitude prediction during events: A test based on previous tsunamis. In *Science of Tsunami Hazards*, 21, 135–143.

Table 1 Tsunami source functions in the Pacific, Atlantic and Indian Oceans.

Source Zone			Tsunami source functions	
No.	**Abbr.**	**Name**	**Line/zone**	**Numbers**
1	ACSZ	Aleutian-Alaska-Canada-Cascadia	BAZYXW	184
2	CSSZ	Central-South American	BAZYX	382
3	EPSZ	East Philippines	BA	44
4	KISZ	Kamchatka-Kuril-Japan Trench-Izu Bonin-Marianas-Yap	BAZYXW	229
5	MOSZ	Manus Ocean Convergence Boundary	BA	34
6	NVSZ	New Britain-Solomons-Vanuatu	BA	74
7	NGSZ	North New Guinea	BA	30
8	NTSZ	New Zealand-Kermadec-Tonga	BA	81
9	NZSZ	South New Zealand	BA	14
10	RNSZ	New Ryukus-Kyushu-Nankai	BA	44
11	KISZ	Kamchatskii-Bering Source Zone	BAZ	13
			Subtotal:	**1129**
12	ATSZ	Atlantic	BA	214
13	SSSZ	South Sandwich	BAZ	33
			Subtotal:	**247**
14	IOSZ	Adaman-Nicobar-Sumatra-Java	BAZY	307
15	MKSZ	Makran	BA	20
16	WPSZ	West Philippines	BA	22
			Subtotal:	**349**
			Total:	**1725**

Table 2 Tsunami sources for past tsunamis.

Earthquake / Seismic info				Tsunami info		
Event	**USGS Date Time (UTC) Epicenter**	**CMT Date Time (UTC) Centroid**	**Magnitude Mw (CMT)**	**Tsunami Magnitude[1]**	**Subduction Zone**	**Tsunami Source**
1946 Unimak	01 Apr 12:28:56 52.75ºN 163.50ºW	n/a	[2]8.5	8.5	Aleutian-Alaska-Cascadia (ACSZ)	7.5 × b23 + 19.7 × b24 + 3.7 × b25
1952 Kamchatka	04 Nov 16:58:26.0 [3]52.76ºN 160.06ºE	n/a	[3]9.0	8.7	Kamchatka-Kuril-Japan-Izu-Mariana-Yap (KISZ)	Tang *et al.* (2006)
1957 Andreanov	09 Mar 14:22:31 51.56ºN 175.39ºW	n/a	[3]8.6	8.7	Aleutian-Alaska-Cascadia (ACSZ)	31.4 × a15 + 10.6 × a16 + 12.2 × a17
1960 Chile	22 May 19:11:14 [3]38.29ºS 73.05ºW	n/a	[4]9.5	n/a	Central-South America (CSSZ)	Kanamori & Ciper (1974)
1964 Alaska	28 Mar 03:36:00 [3]61.02ºN 147.65ºW	n/a	[3]9.2	8.9	Aleutian-Alaska-Cascadia (ACSZ)	15.4 × a34+19.4×a35+ 48.3 × z34+18.3×b34+15.1×b35
1994 East Kuril	04 Oct 13:22:58 43.73ºN 147.321ºE	04 Oct 13:23:28.5 43.60ºN 147.63ºE	8.3	8.1	Kamchatka-Kuril-Japan-Izu-Mariana-Yap (KISZ)	9.0 x a20
1996 Andreanof	10 Jun 04:03:35 51.56ºN 175.39ºW	10 Jun 04:04:03.4 51.10ºN 177.410ºW	7.9	7.8	Aleutian-Alaska-Cascadia (ACSZ)	2.4 x a15 + 0.8 x a16
2003 Hokkaido	25 Sep 19:50:06 41.775ºN 143.904ºE	25 Sep 19:50:38.2 42.21ºN 143.84ºE	8.3	8.0	Kamchatka-Kuril-Japan-Izu-Mariana-Yap (KISZ)	3.6m × (100 × 100km) 109#rake, 20#dip, 230#strike, 25 m depth
2003 Rat Island	17 Nov 06:43:07 51.13ºN 178.74ºE	17 Nov 06:43:31.0 51.14ºN 177.86ºE	7.7	7.8	Aleutian-Alaska-Cascadia (ACSZ)	[5]2.81 × b11
2006 Tonga	03 May 15:26:39 20.13ºS 174.161ºW	03 May 15:27:03.7 20.39ºS 173.47ºW	8.0	8.0	New Zealand-Kermadec-Tonga (NTSZ)	6.6 × b29 (Tang *et al*., 2008b)
2006 Kuril	15 Nov 11:14:16 46.607ºN 153.230ºE	15 Nov 11:15:08 46.71ºN 154.33ºE	8.3	8.1	Kamchatka-Kuril-Japan-Izu-Mariana-Yap (KISZ)	[5]4.0x a12+0.5 xb12+ 2.0 xa13+ 1.5 xb13 (Titov, 2009)
2007 Kuril	13 Jan 04:23:20 46.272ºN 154.455ºE	13 Jan 04:23:48.1 46.17ºN 154.80ºE	8.1	7.8	Kamchatka-Kuril-Japan-Izu-Mariana-Yap (KISZ)	-3.2 × b13
2007 Solomon	01 Apr 20:39:56 8.481ºS 156.978ºE	01 Apr 20:40:38.9 7.76ºS 156.34ºE	8.1	8.2	New Britain-Solomons-Vanuatu (NVSZ)	12.0 × b10
2007 Peru	15 Aug 23:40:57 13.354ºS 76.509ºW	15 Aug 23:41:57.9 13.73ºS 77.04ºW	8.0	8.3	Central-South America (CSSZ)	3.6×a62+5.7×z63+5.3×b62
2009 Samoa	29 Sep 17:48:10 15.509ºS 172.034ºW	29 Sep 17:48:26.8 15.13ºS 171.97ºW	8.1	8.2	New Zealand-Kermadec-Tonga (NTSZ)	a34×6.4+3.2×c35

[1] Preliminary source – derived from tsunami source functions and deep-ocean observations
[2] López and Okal (2006)
[3] United States Geological Survey (USGS)
[4] Kanamori and Ciper (1974)
[5] Tsunami source was obtained in real time and applied to the forecast

2010 Chile	27 Feb 06:34:14 35.909ºS 72.733ºW	27 Feb 06:35:15.4 35.95ºS 73.15ºW	8.8	8.8	Central-South America (CSSZ)	a87× 9.68+z88 ×24.5+a88×15.35+a91× 13.19+z92×24.82
2011 Japan	11 March 05:46:23 38.322ºN 142.369 E	11 March 05:47:32.8 37.52ºS 143.05 E	9.1	8.8	Kamchatka-Kuril-Japan-Izu-Mariana-Yap (KISZ)	[5]4.66× b24 + 12.23 ×b25+26.31× a26+21.27×b26+22.75 ×a27+4.98× b27 (Tang *et al*., 2011)
2012 Queen Charlotte Islands	28 October 03:04:09 52.742ºN 132.131ºW	28 October 03:04:39.2 52.47ºN 132.13ºW	7.7	7.9	Aleutian-Alaska-Cascadia (ACSZ)	0.36×52b+4.3×51a

Table 3 MOST setups of Keauhou reference and forecast models.

Grid	Region	Reference Model				Forecast model		
		Coverage Lon. (^{0}E) Lat. (^{0}N)	Cell Size (")	Time Step (sec)		Coverage Lon. (^{0}E) Lat. (^{0}N)	Cell Size (")	Time Step (sec)
A	Hawaii	199.0 - 205.98 18.0 – 23.0	36 (699 x 500)	3	A	199 - 205.9667 18.0317 - 22.9983	120 (210 x 150)	11.05
B	Big Island	202.8483-205.3983 18.6933 - 21.4283	6 (1531 x 1642)	0.45	B	203.8200 - 204.1983 19.3358 - 20.3091	6 (228 x 585)	0.85
C	Keauhou	203.9689 -204.070 19.4983 - 19.6642	1/3 (1729 x 487)	0.15	C	204.0166 - 204.0410 19.5497 - 19.6122	1 (89 x 226)	0.85
Minimum offshore depth (m)		1				1		
Water depth for dry land (m)		0.1				0.1		
Manning coefficient		0.025				0.03		
Computational time for a 4-hr simulation		~ 12 hours				**14 minutes**		

Table 4 Sources of the 18 Mw 9.3 synthetic tsunamis and model results at the Keauhou warning point computed by the reference and forecast models.

No.	Subd. Source Zone	alpha	Ref. model η_{max} (m)	Ref. model t_{max} (hour)	Forecast Model η_{max} (m)	Forecast Model t_{max} (hour)	Location
1	KISZ AB	22-31	3.57	7.999	3.03	8.004	Japan
2	KISZ AB	1-10	2.66	8.049	1.78	8.036	Kamchatka
3	ACSZ AB	16-25	1.71	5.349	1.22	4.882	Central Aleutian
4	ACSZ AB	22-31	0.75	5.117	0.64	5.099	Unimak
5	ACSZ AB	50-59	1.10	6.899	1.59	6.662	Canada
6	ACSZ AB	56-65	0.87	7.416	0.92	6.681	Cascadia
7	CSSZ AB	1-10	0.32	11.717	0.25	17.448	Central American
8	CSSZ AB	41-50	0.29	12.299	0.29	12.289	Columbia-Ecuador
9	CSSZ AB	86-95	0.77	16.133	0.72	16.085	Chile
10	CSSZ AB	100-109	2.25	16.899	2.13	16.373	Southern Chile
11	NTSZ AB	20-29	0.59	7.950	0.62	10.665	Tonga
12	NTSZ AB	30-39	2.37	5.867	2.32	5.869	Northern Tonga
13	NVSZ AB	28-37	1.04	8.033	1.01	8.033	Vanuatu
14	MOSZ AB	1-10	1.11	8.300	1.07	8.327	Manus
15	NGSZ AB	3-12	0.69	14.133	0.23	9.948	New Guinea
16	EPSZ AB	6-15	1.90	11.767	1.52	11.774	East Philippines
17	RNSZ AB	12-21	0.89	10.566	0.73	10.569	Nankai
18	KISZ AB	32-41	2.34	9.200	1.65	8.288	Izu

Appendix A.

The following appendix lists the input files for Keauhou developed in 2011.

A1. Reference model *.in file for Keauhou , Hawaii for MOST version 4.0

A.
0.001 Minimum amplitude of input offshore wave (m):
1 Input minimum depth for offshore (m)
0.1 Input "dry land" depth for inundation (m)
0.0009 Input friction coefficient (n**2)
2 Number of grids
2 Interpolation domain for outer boundary
2 inner boundary
RA_hawaii_36s_20070806.nc
RB_kawaihae_B6s_20070806.nc
1
3 Input time step (sec)
9600 Input amount of steps
0 COntunue after input stops
20 Input number of steps between snapshots
1 saving inner boundaries every n-th timestep
1 ...Saving grid every n-th node, n=
./
/home/tg23/data/tang/store_c2/pacific_prop_db/2003_Hokkaido/sim_src/

B
0.002 Minimum amplitude of input offshore wave (m):
-300 Input minimum depth for offshore (m)
0.1 Input "dry land" depth for inundation (m)
0.0009 Input friction coefficient (n**2)
2 Number of grids
2 Interpolation domain for outer boundary
2 inner boundary
RB_kawaihae_B6s_20070806.nc
RC_keauhou_10m.nc
1
0.45 Input time step (sec)
64000 Input amount of steps
0 COntunue after input stops
133 Input number of steps between snapshots
1 saving inner boundaries every n-th timestep
1 ...Saving grid every n-th node, n=
./
./

C
0.002 Minimum amplitude of input offshore wave (m):
-300 Input minimum depth for offshore (m)
0.1 Input "dry land" depth for inundation (m)
0.0009 Input friction coefficient (n**2)

```
1        Number of grids
2         Interpolation domain for outer boundary
2         inner boundary
RC_keauhou_10m.nc
2
0.15      Input time step (sec)
192000    Input amount of steps
0             COntunue after input stops
400    Input number of steps between snapshots
1      saving inner boundaries every n-th timestep
1       ...Saving grid every n-th node, n=
./
./
```

A2. Forecast model *.in file for Keauhou, Hawaii for MOST version 2.0

```
0.0001    Minimum amplitude of input offshore wave (m):
1         Input minimum depth for offshore (m)
0.1       Input "dry land" depth for inundation (m)
0.000625  Input friction coefficient (n**2)
1         runup flag for grids A and B (1=yes,0=no)
300.0     blowup limit
0.85      Input time step (sec)
21176     Input amount of steps
13        Compute "A" arrays every n-th time step, n=
1         Compute "B" arrays every n-th time step, n=
26        Input number of steps between snapshots
1      ...Starting from
1       ...Saving grid every n-th node, n=
hawaii_2min_20070806.asc.s.c
FB_keauhou_6s2_20110602.most
FC_Keauhou_1s3_20110512.c
/home/tg23/data/tang/src_nc/src_sim_test/hawa/
./
1 1 1 1
1
1 76 183  keauhou 204.03740740  19.5616666 depth  m: 3.60
```

List of Figures

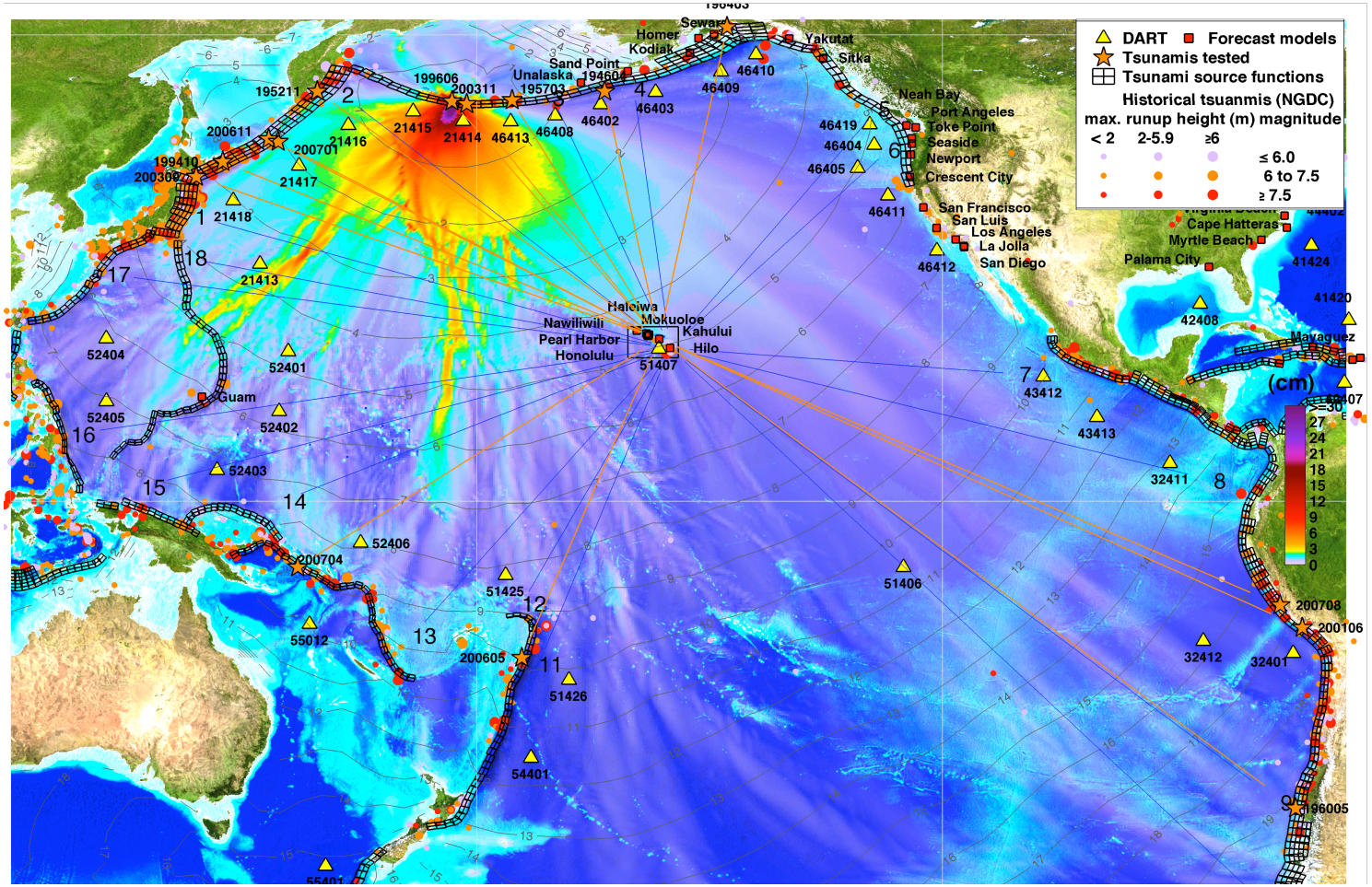

Figure 1: Overview of the Tsunami Forecast System in Pacific. System components include DART system (yellow triangles), pre-computed tsunami source function (unfilled black rectangles) and high-resolution forecast models (red squares). Colors show the offshore forecast of the computed maximum tsunami amplitude in cm for the 17 November 2003 Rat Islands tsunami in the Pacific. Contours indicate the travel time in hours. ——, seventeen past tsunamis and——, eighteen simulated magnitude 9.3 tsunamis tested in this study.

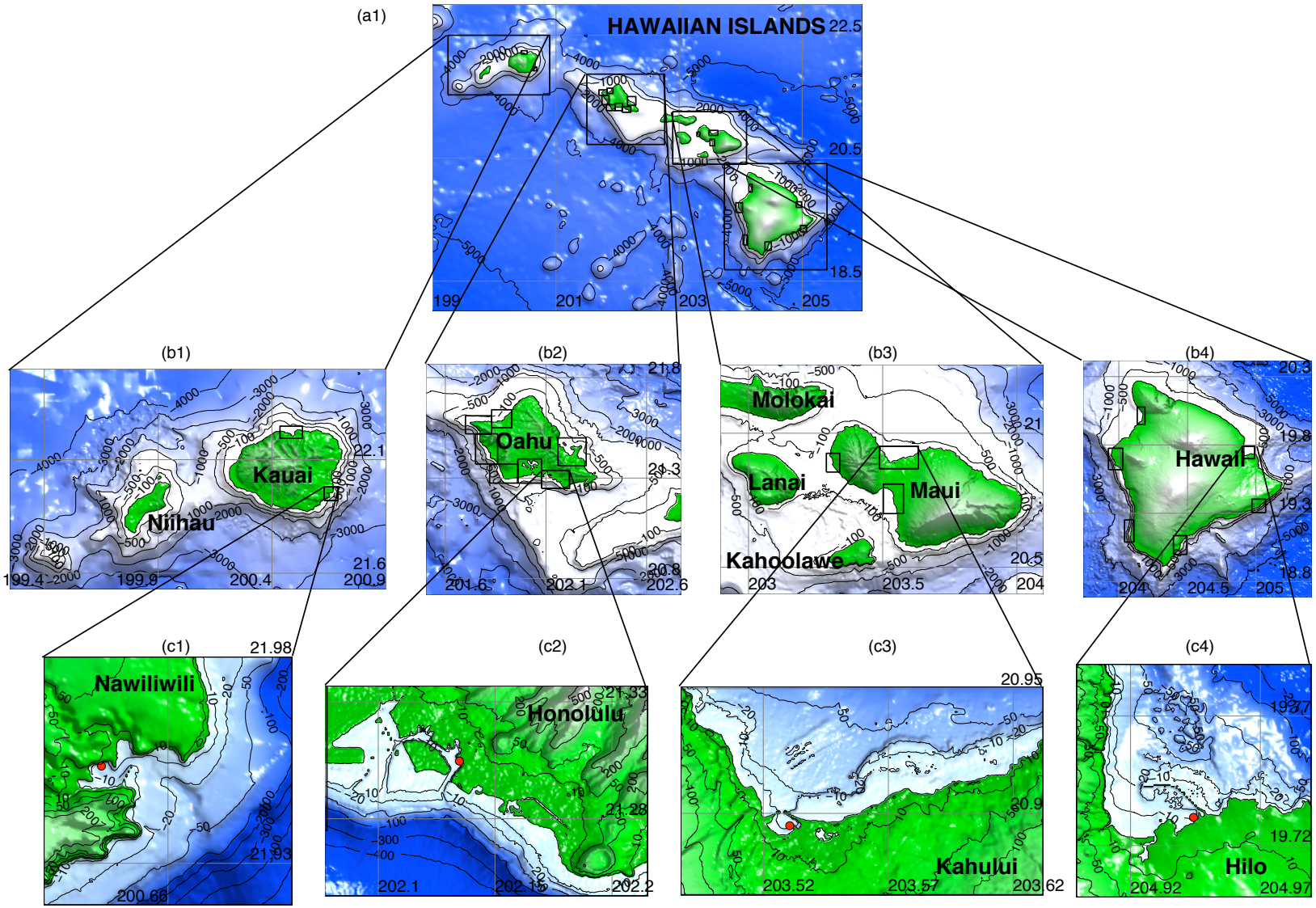

Figure 2: Forecast model setups for several forecast sites in Hawaii: (a) 2-arc-min (~3600m) regional, (b) 12-18-arc-sec (~360-540m) intermediate and (c) 2-arc-sec (~60m) nearshore grids for Nawiliwili, Honolulu, Kahului and Hilo. Red dots, coastal tide stations; red pluses, offshore locations.

Figure 3: An aerial photo of Keauhou (Image courtesy http://www.soest.hawaii.edu/coasts

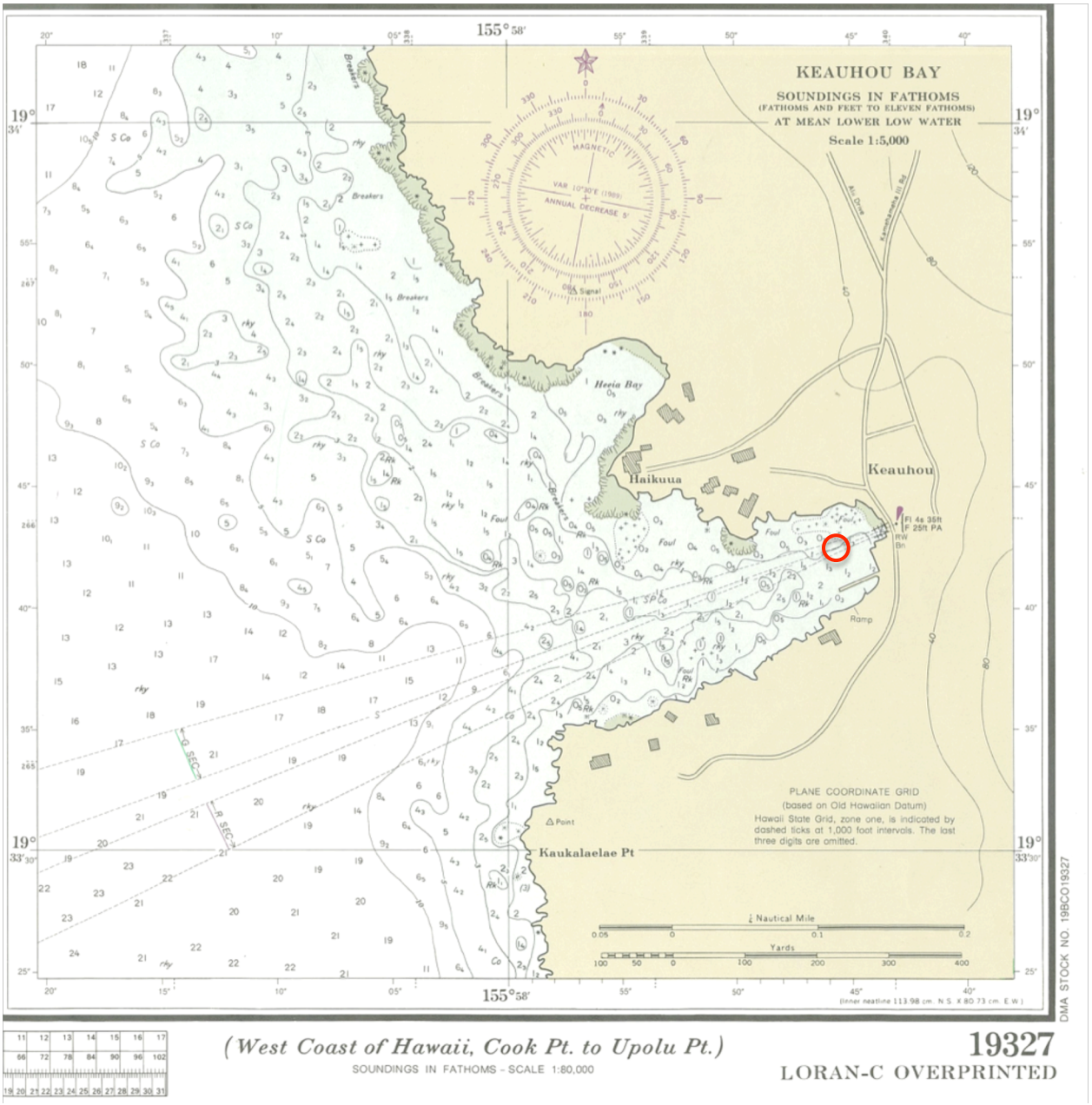

Figure 4: A chart of Keauhou (NOAA Chart 19327). Soundings in fathoms at Mean Lower Low Water. Contour and summit elevation values ate in feet above Mean Sea Level. Red Circle, Keauhou warning point.

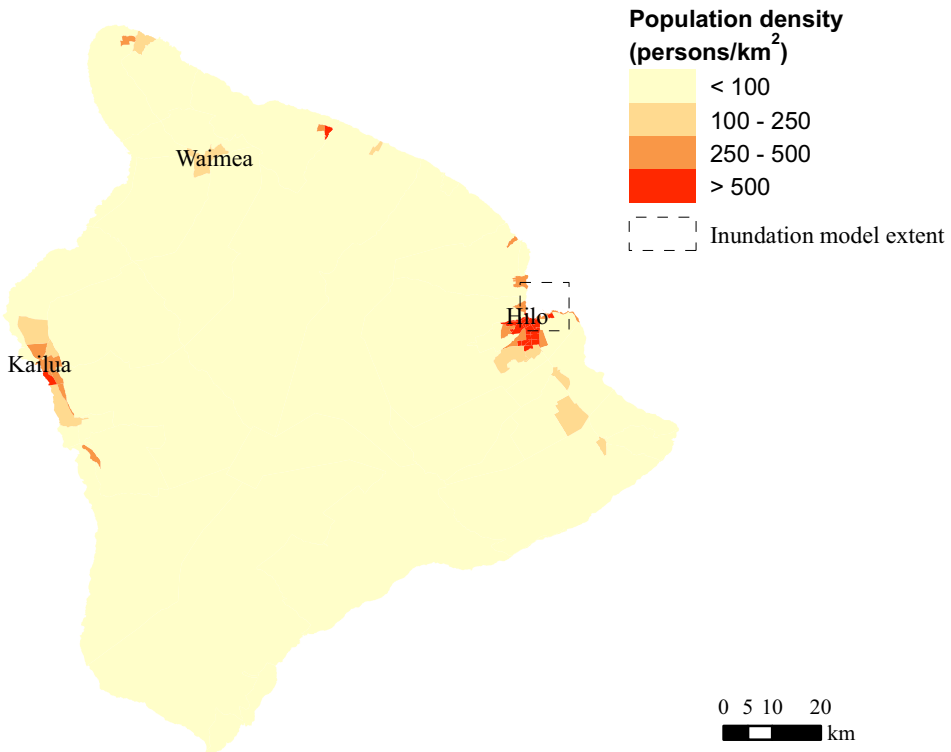

Figure 5: Population density, Hawaii. (Source: 2000Census)

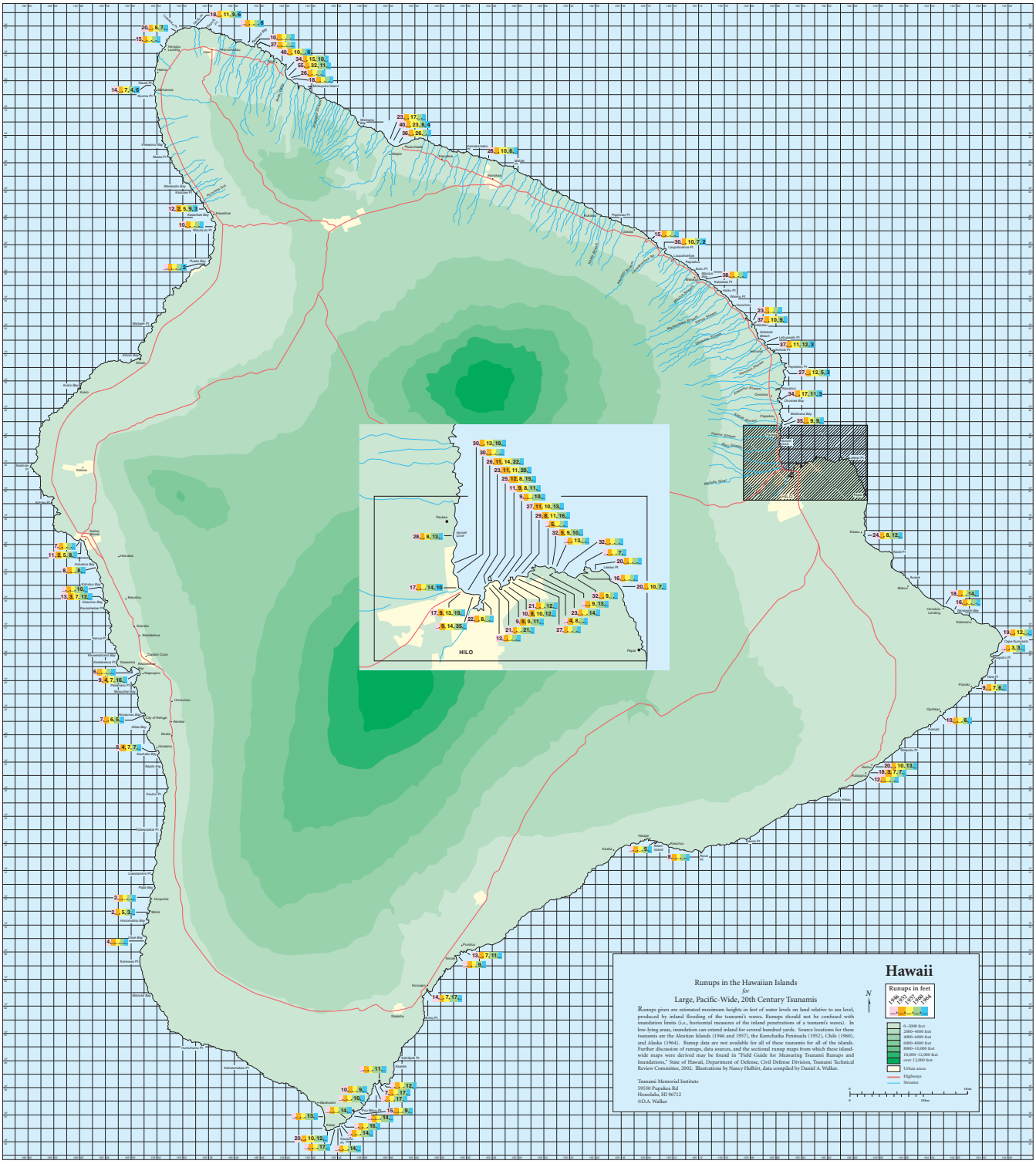

Figure 6: Run-ups in the Island of Hawaii for the 1946, 1957, 1960 and 1964 tsunamis (Image from Walker, 2004).

(a)

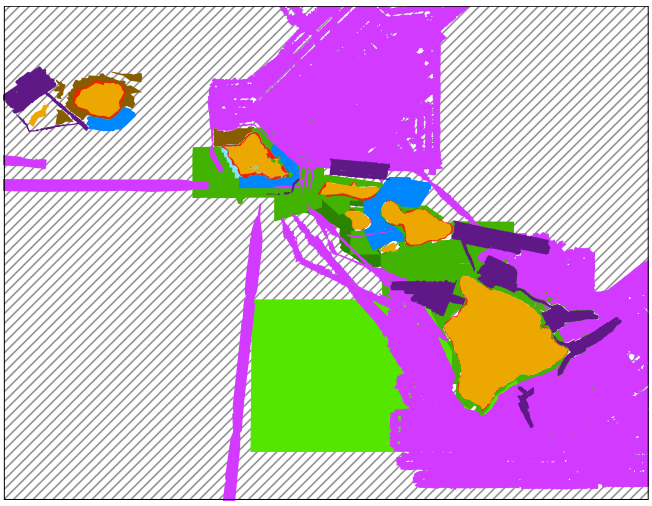

SHOALS LIDAR
JAMSTEC multibeam
MBARI multibeam
Navy multibeam
NOS digital echosounder
NOS multibeam
NOS lead-line surveys
USACE digital echosounder
USGS Seafloor Mapping Project multibeam
NOS nautical chart digitized contours
USGS GLORIA tracklines/Smith & Sandwell
NOAA CSC IfSAR topography
USGS National Elevation Dataset topography

(b)

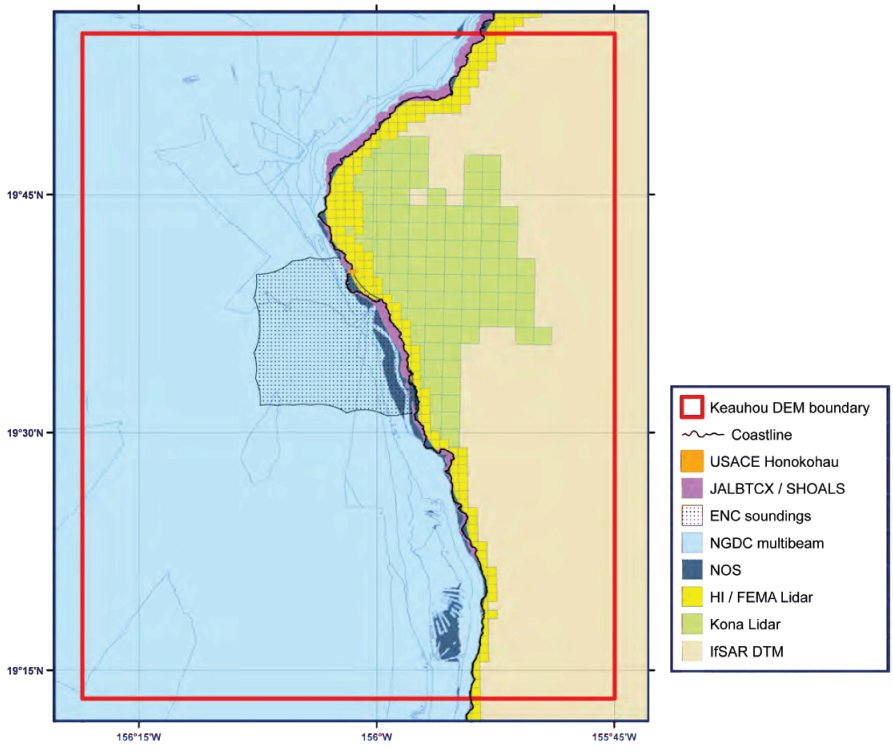

Figure 7: Bathymetric and topographic data source overview. (a) 6 arc-sec (~180m) Hawaii DEM developed at NCTR; (b) 1/3" (~10m) Keauhou DEM developed by NGDC (Image courtesy Carignan et al., 2011).

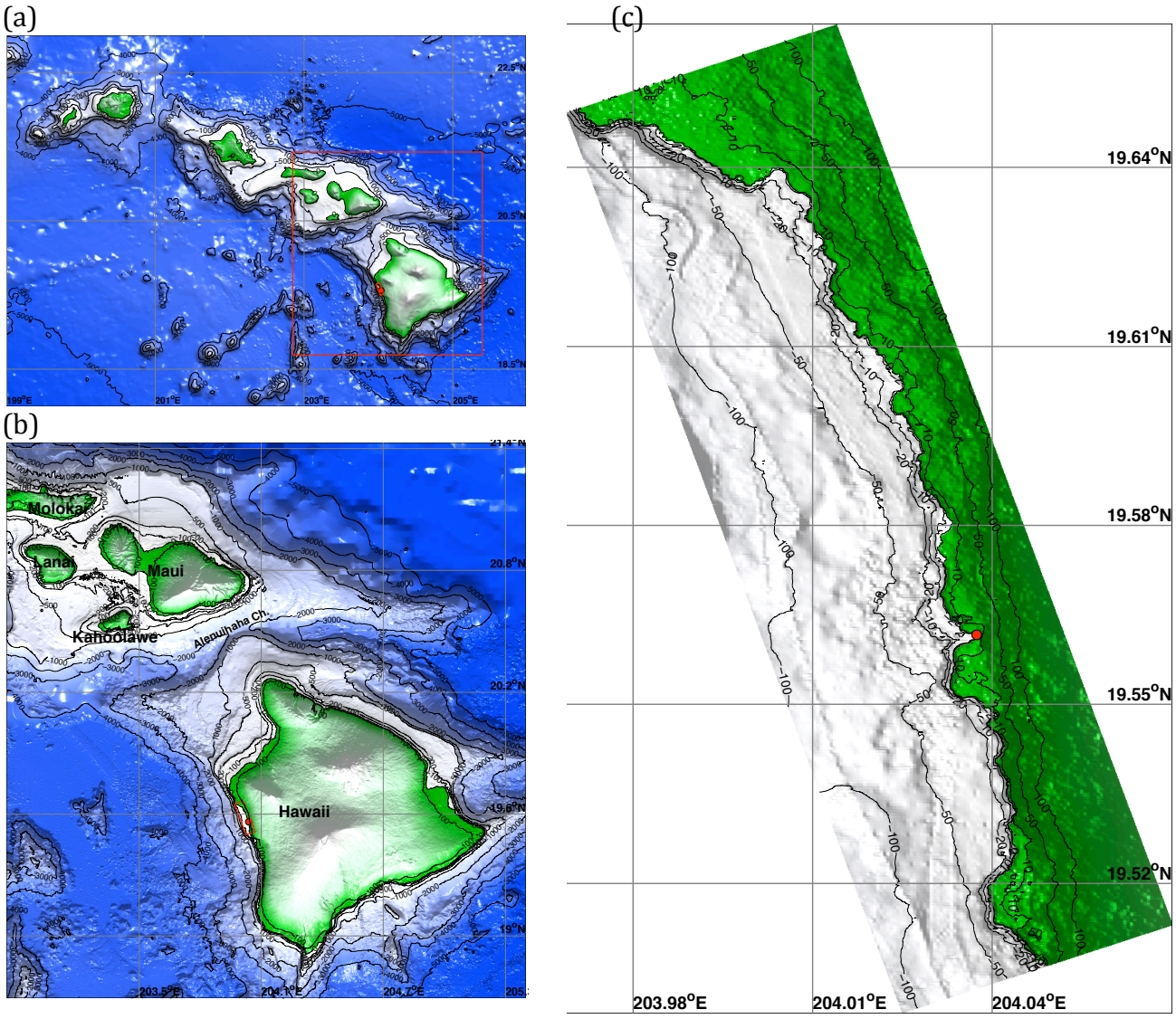

Figure 8: Grid setup of the Keauhou reference model with resolutions of (a) 36" (1080m), (b) 6" (180m),(c) 2" (60m) and (d) 1/3" (10m). □, nested grid boundary; ● Keauhou warning point .

(a)

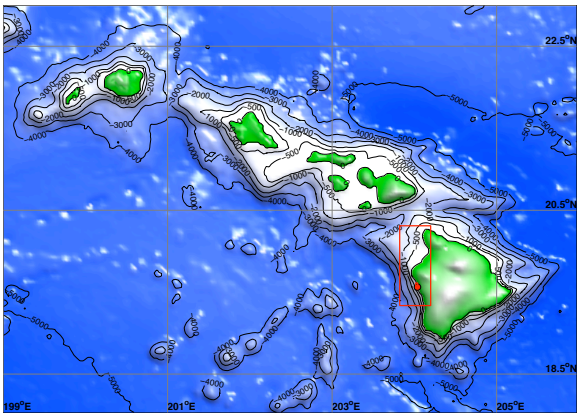

(b)

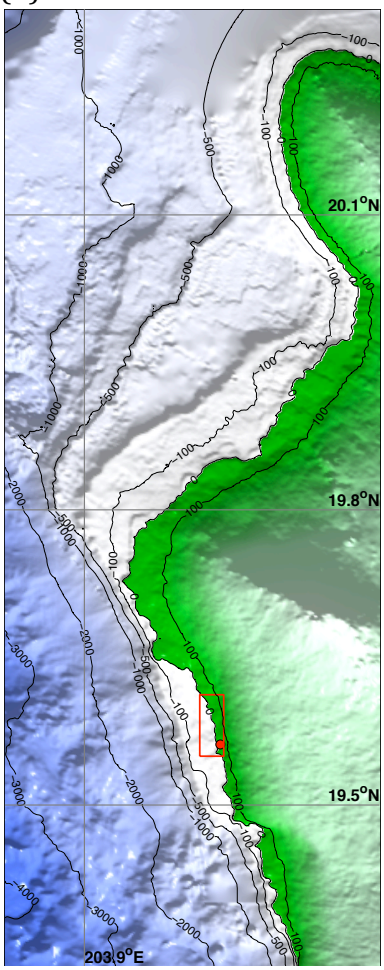

(c)

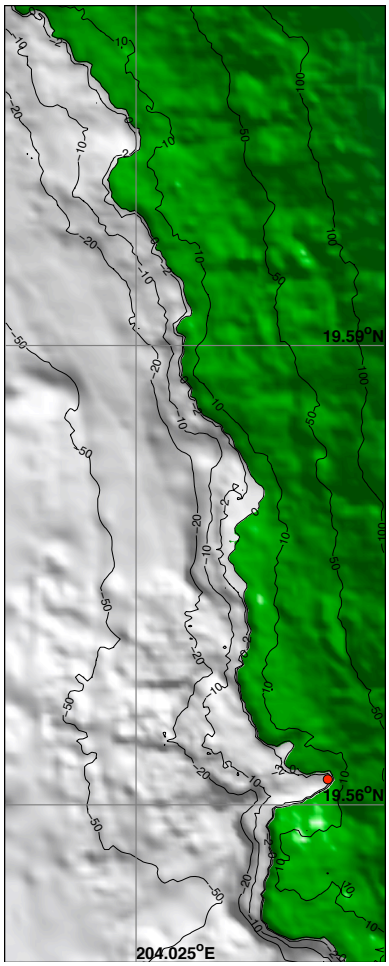

Figure 9: Grid setup of the Lahaina forecast model with resolutions of (a) 120" (3600m), (b) 6" (180m) and (c) 1" (30m). □, nested grid boundary; ●, Keauhou warning point at 204.03740740°E, 19.5616666°N, water depth of 3.5 m.

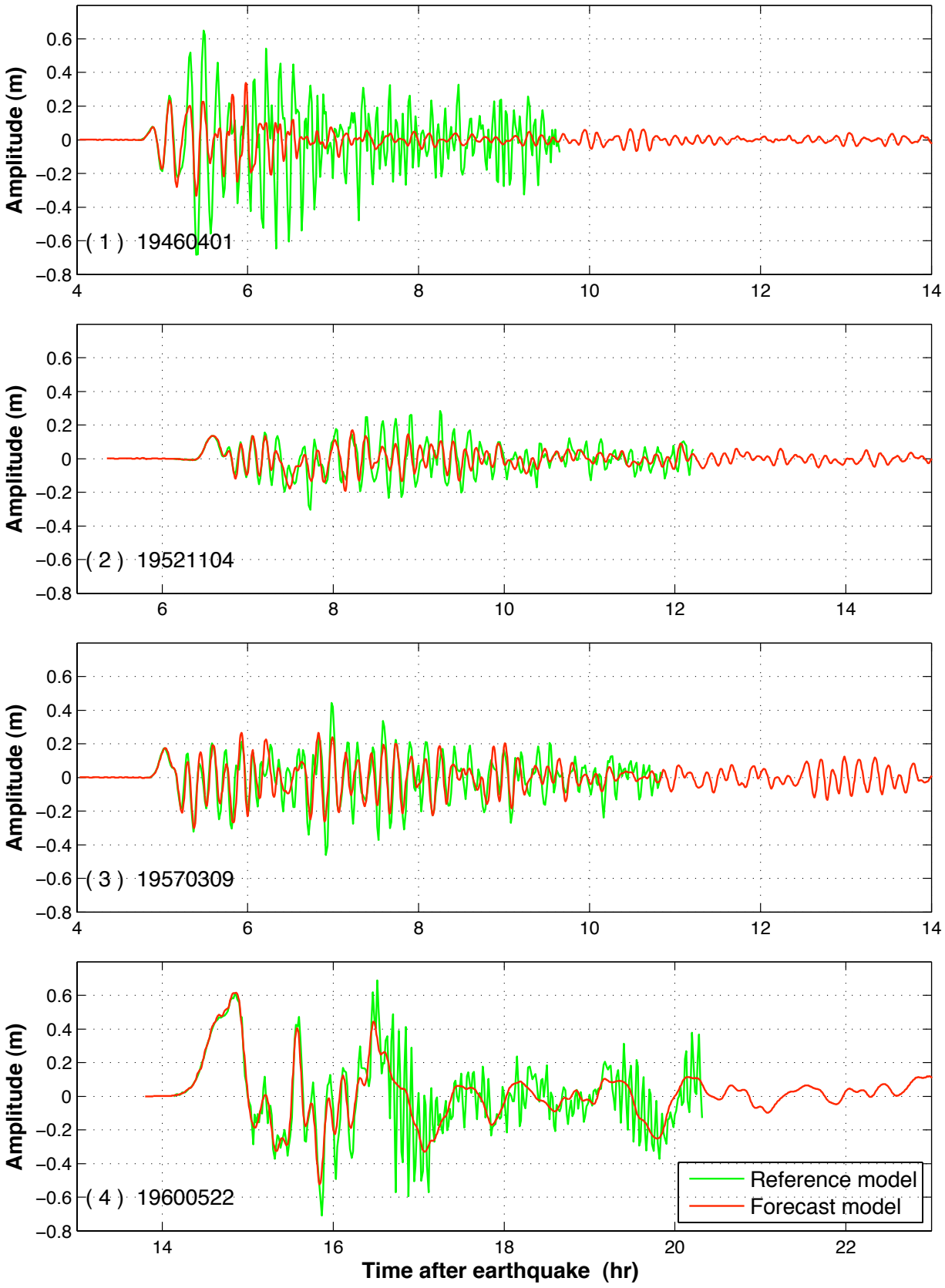

Figure 10: Modeled time series of wave amplitudes at Keauhou warning point for the past 17 tsunamis.

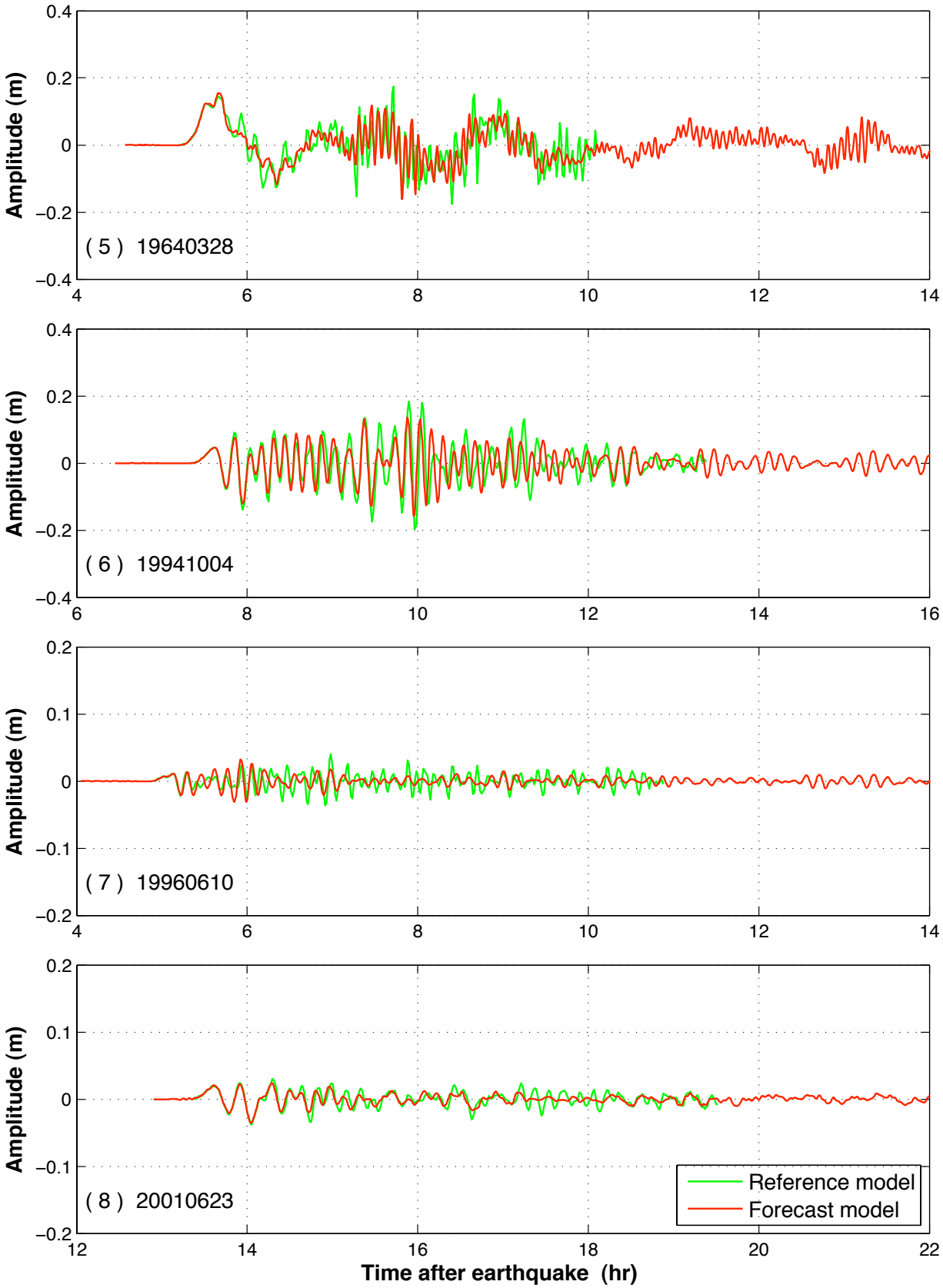

Figure 10: (Continued).

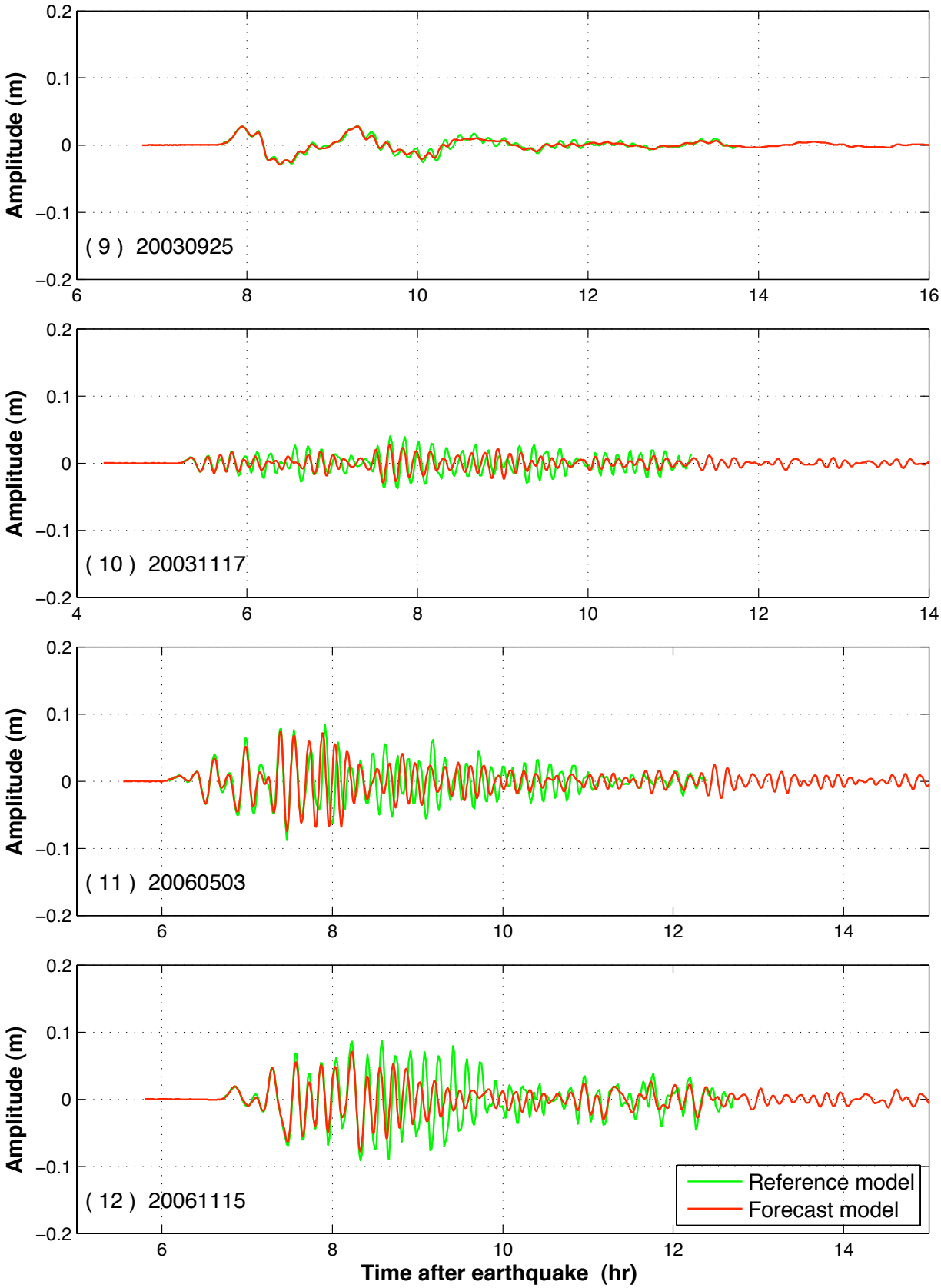

Figure 10: (Continued).

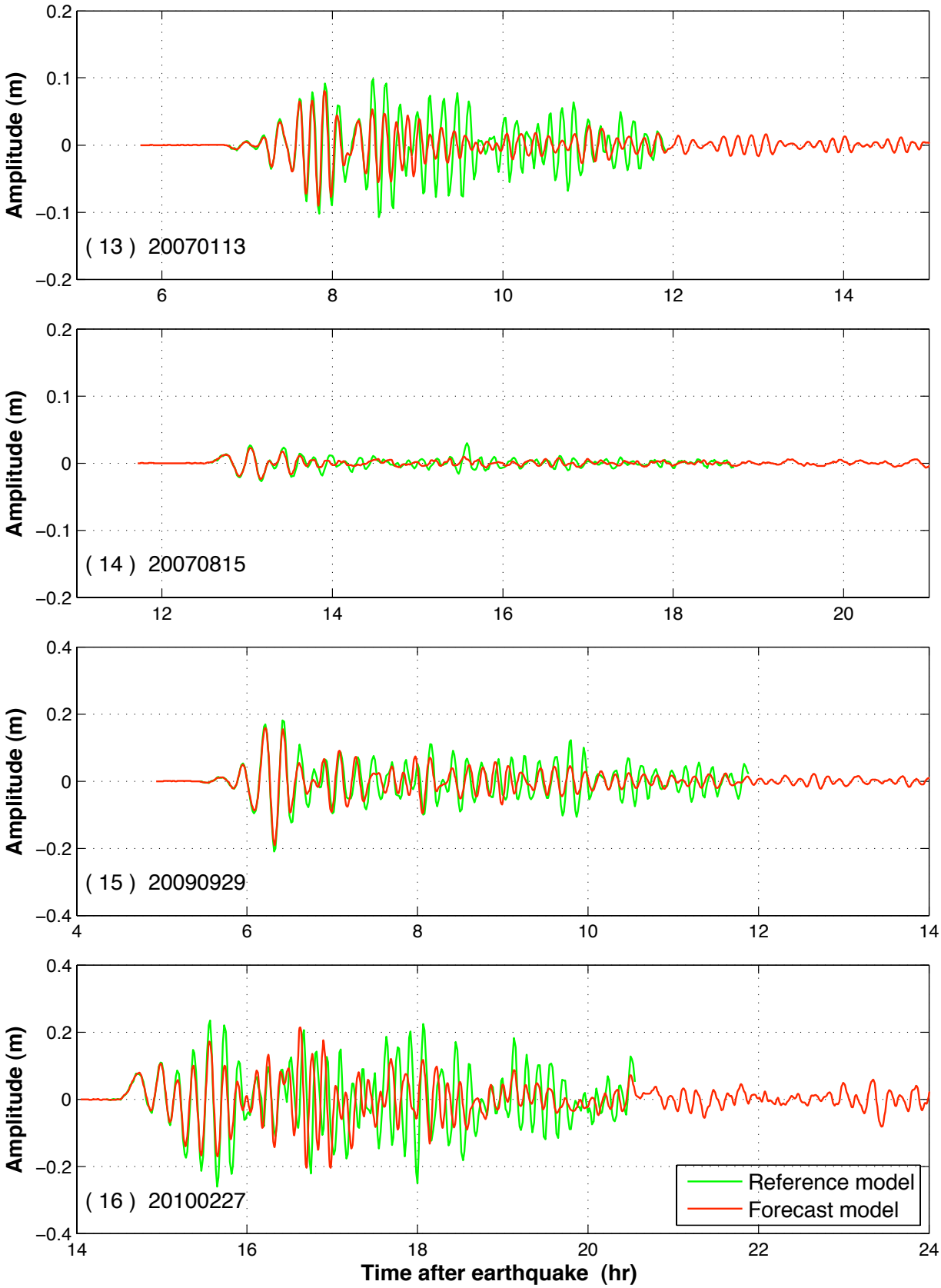

Figure 10: (Continued).

Figure 10: (Continued).

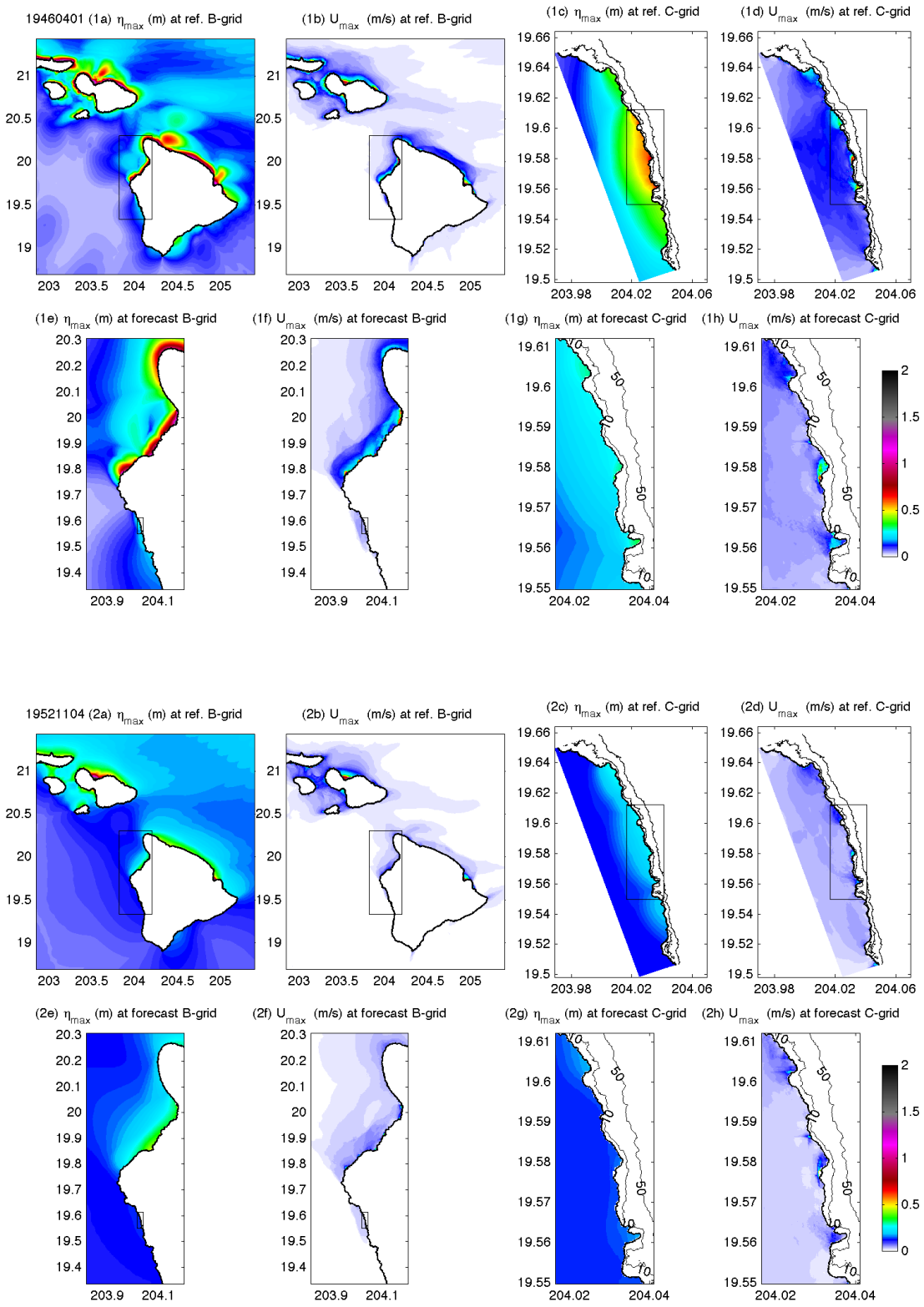

Figure 11: (1-2) Maximum sea surface elevation and current speed computed by the Keauhou reference and forecast models for the (1) 1946 Unimak and (2) 1952 Kamchtka tsunamis.

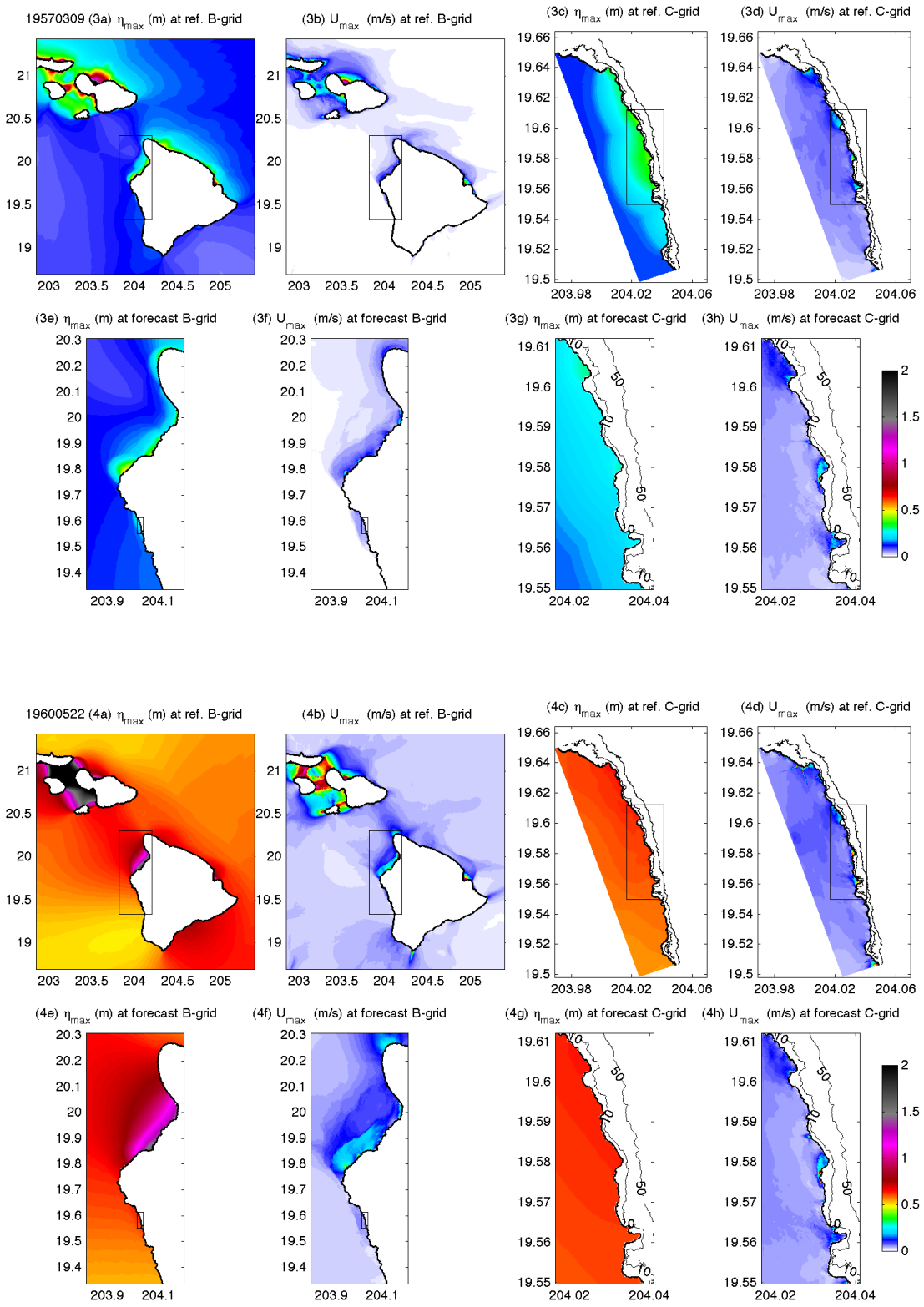

Figure 11 (Continued): (3-4) Computed maximum sea surface elevation and current speed by the Keauhou reference and forecast models for the (3) 1957 Andreanov and (4) 1960 Chile tsunamis.

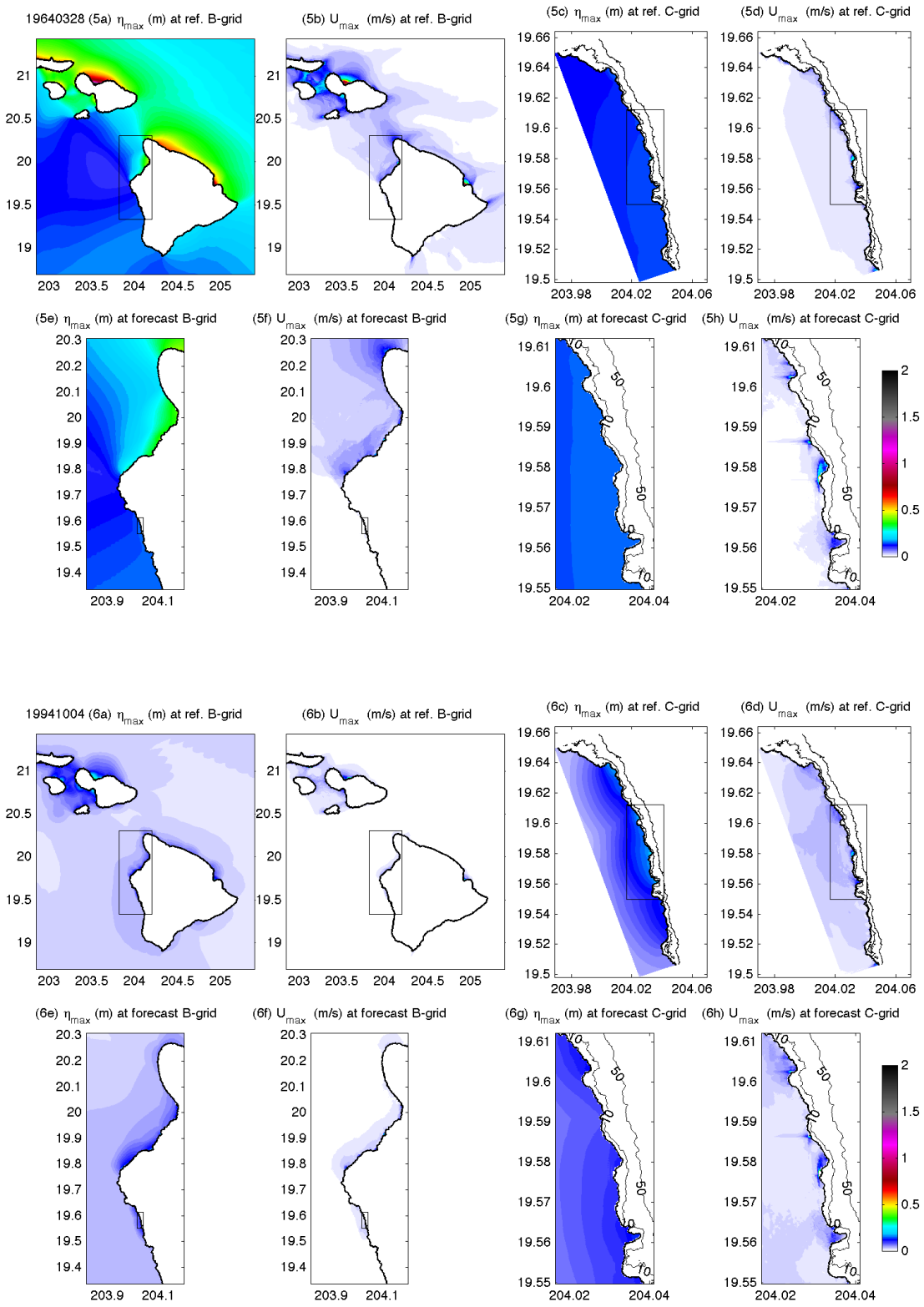

Figure 11 (Continued): (5-6) Computed maximum sea surface elevation and speed by the Keauhou reference and forecast models for the (5) 1964 Alaska and (6) 1994 Kuril Islands tsunamis.

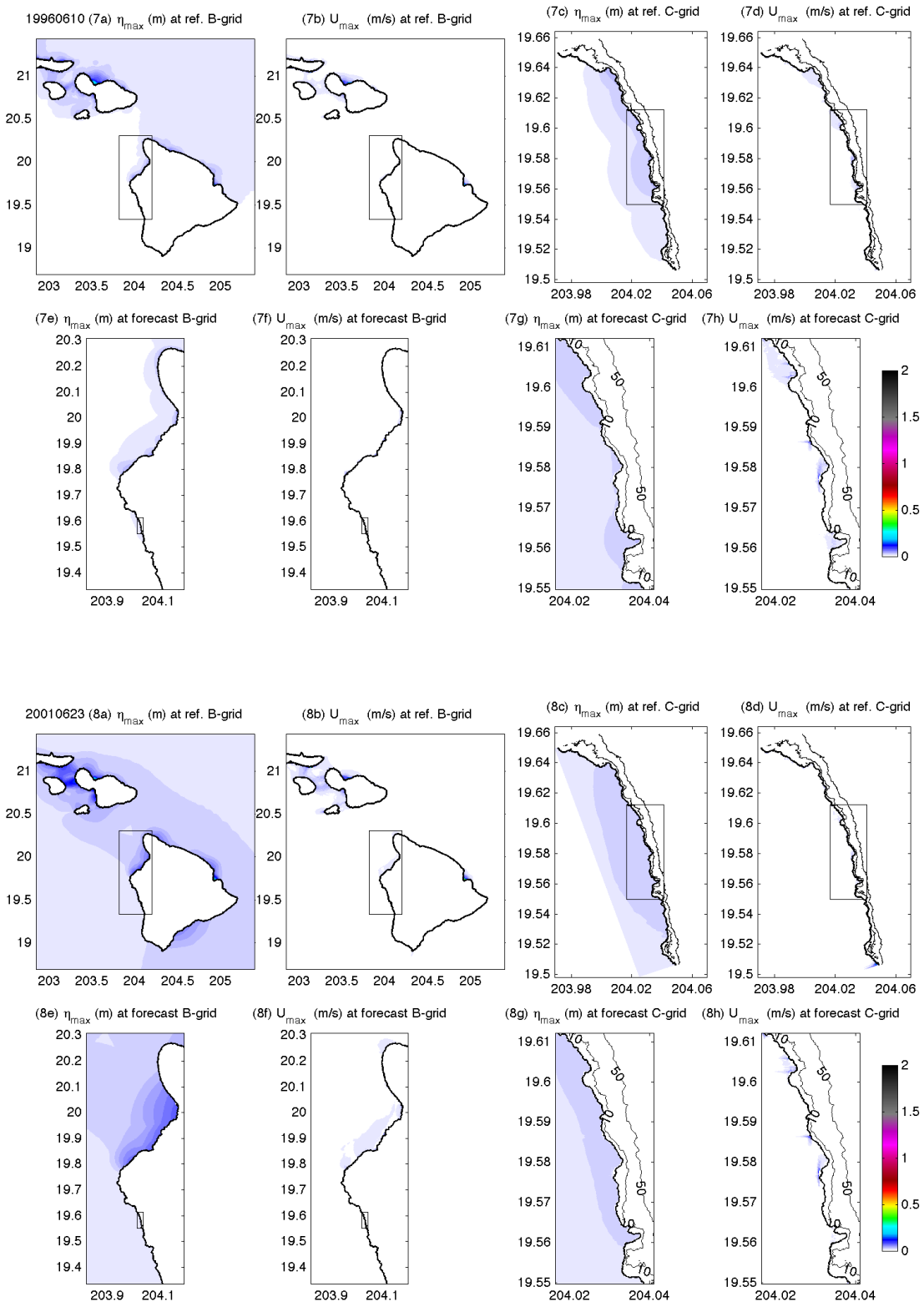

Figure 11 (Continued): (7-8) Computed maximum sea surface elevation and speed by the Keauhou reference and forecast models for the (7) 1996 Andreanov and (8) 2001 Peru tsunamis.

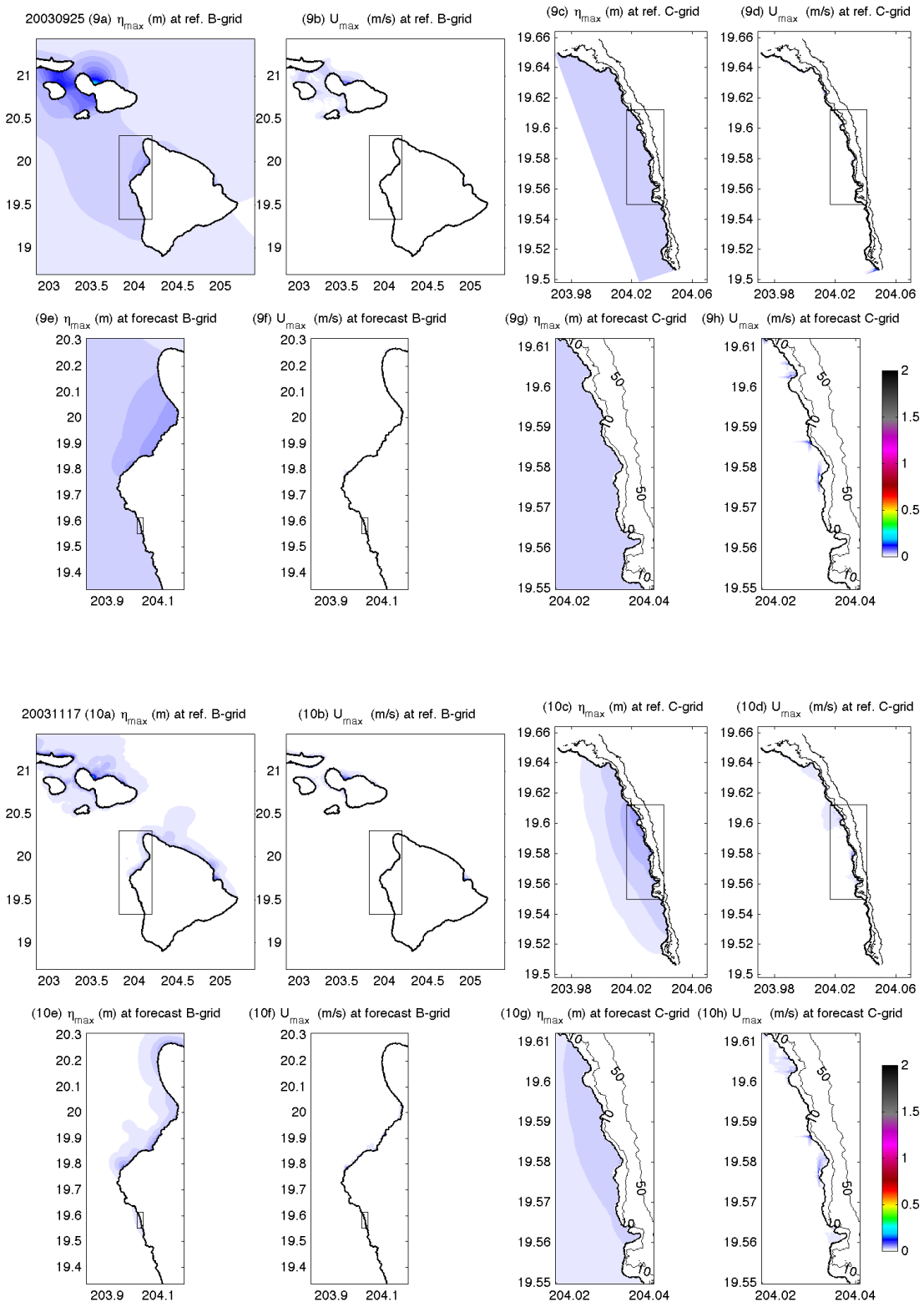

Figure 11 (Continued): (9-10) Computed maximum sea surface elevation and speed by the Keauhou reference and forecast models for the (9) 2003 Hokkaido and (11) 2003 Rat Island tsunamis.

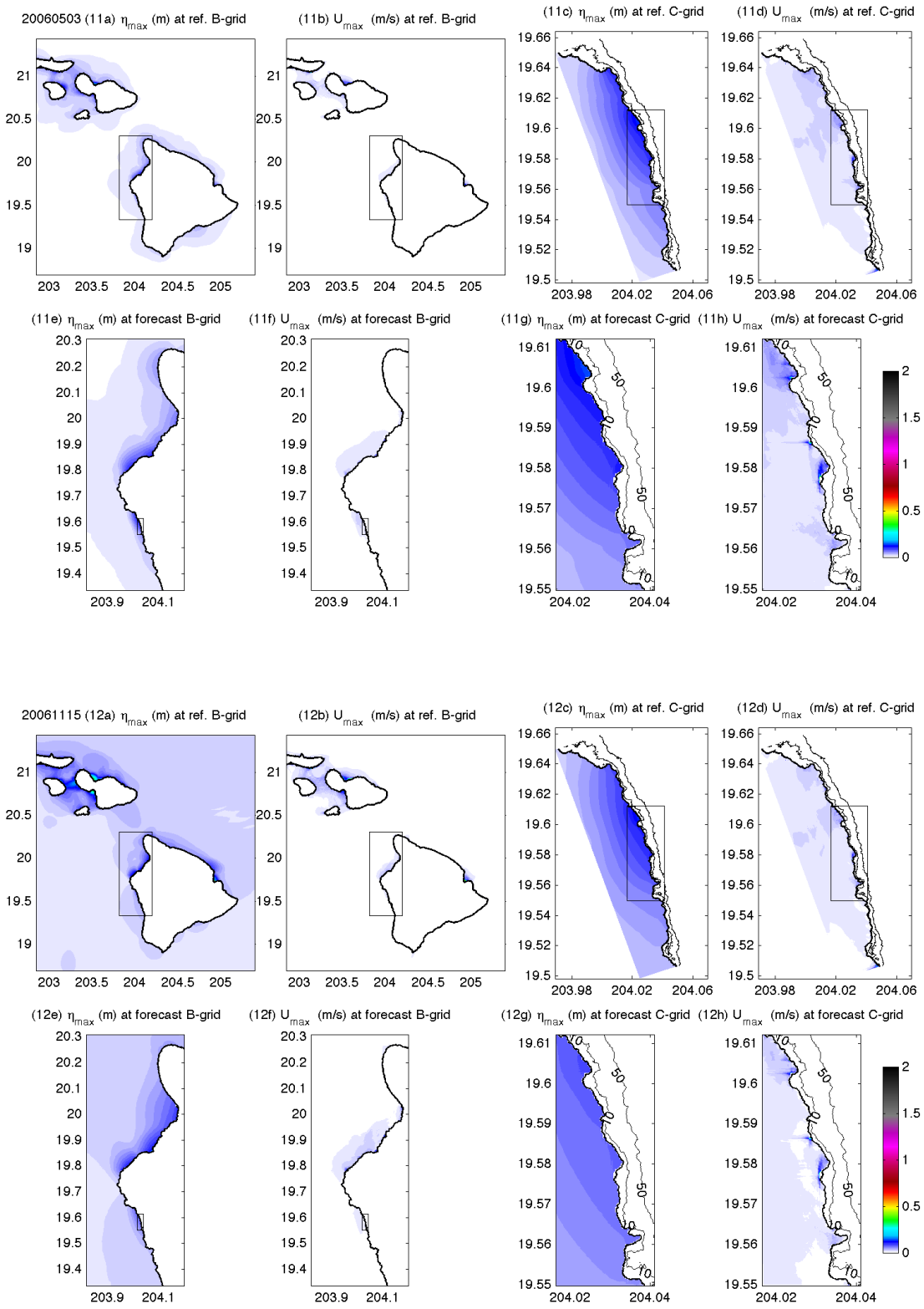

Figure 11 (Continued): (11-12) Computed maximum sea surface elevation and speed by the Keauhou reference and forecast models for the (11) 2006 Tonga and (12) 2006 Kuril Islands tsunamis.

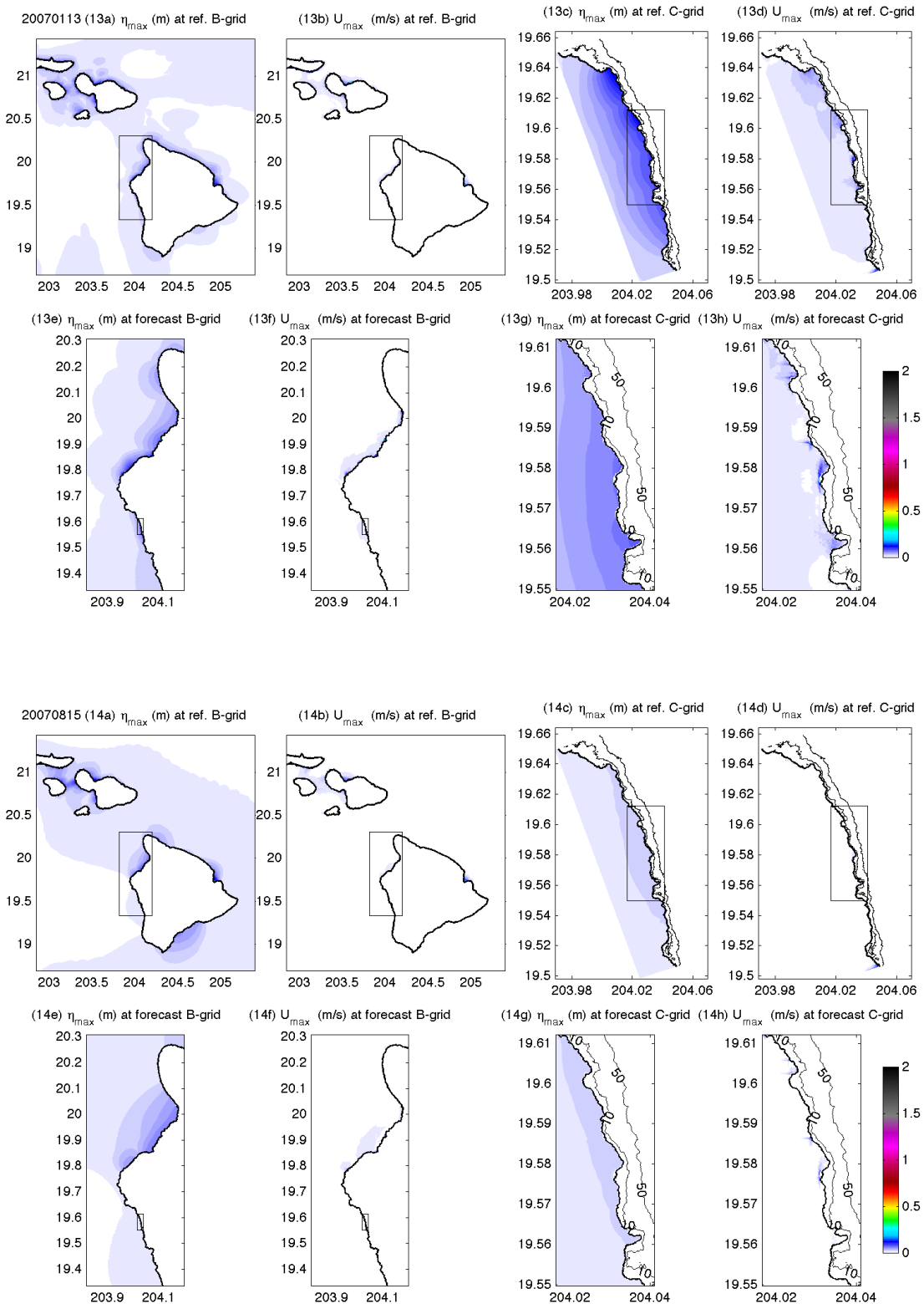

Figure 11 (Continued): (13-14) Computed maximum sea surface elevation and speed by the Keauhou reference and forecast models for the (13) 2007 Kuril Islands and (14) 2007 Peru tsunamis.

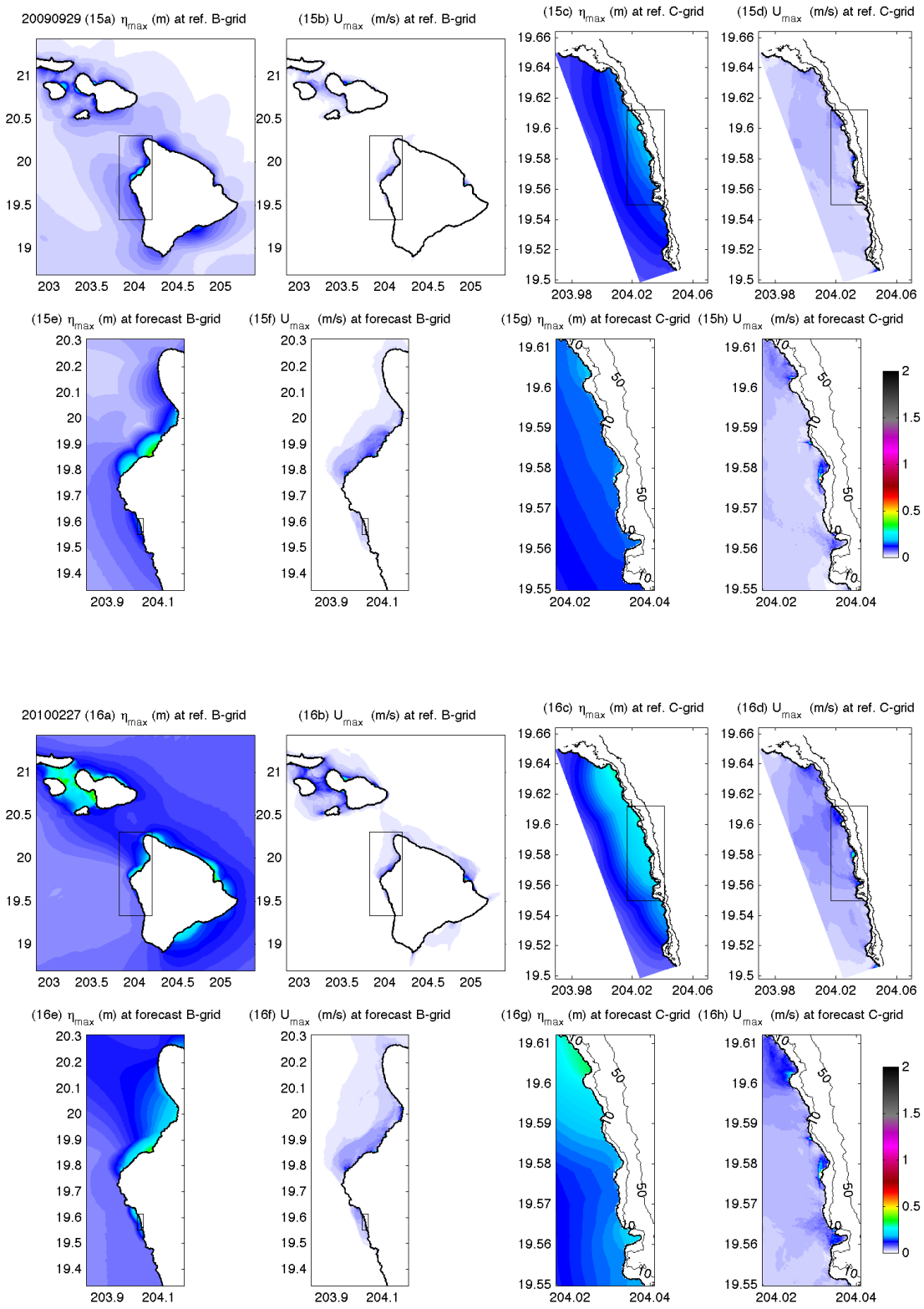

Figure 11 (Continued): (15-16) Computed maximum sea surface elevation and speed by the Keauhou reference and forecast models for the (15) 2009 Samoa and 2010 Chile tsunamis

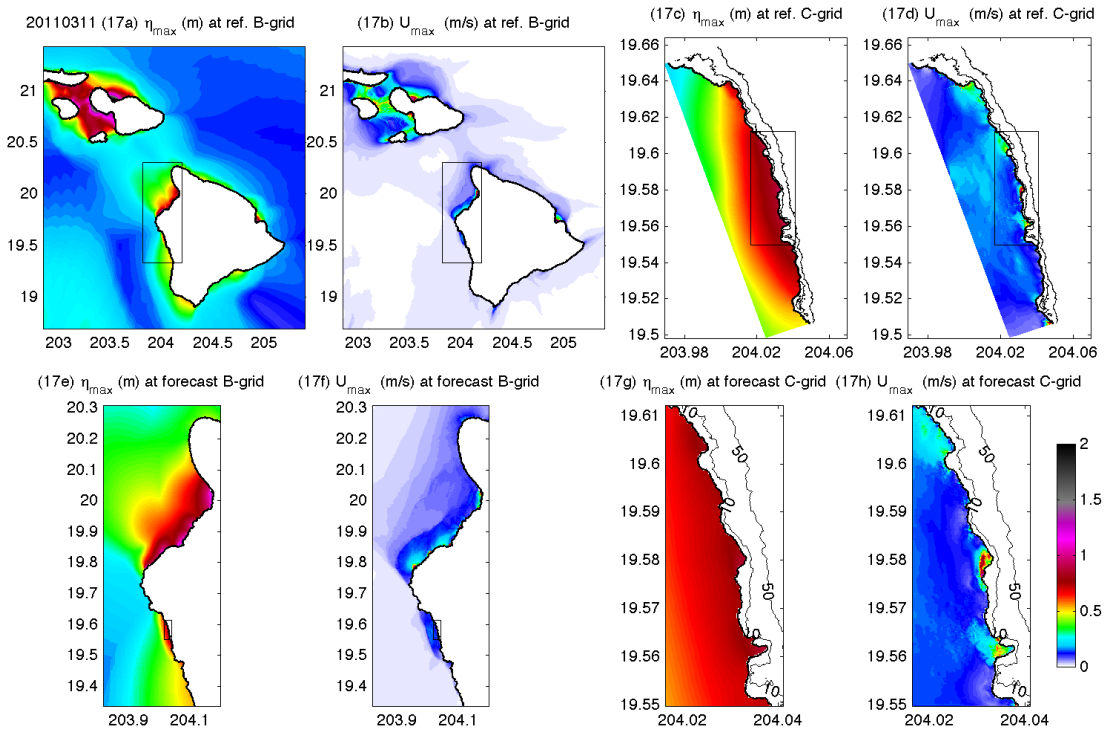

Figure 11 (Continued): (17) Computed maximum sea surface elevation and speed by the Keauhou reference and forecast models for the 2011 Japan tsunamis

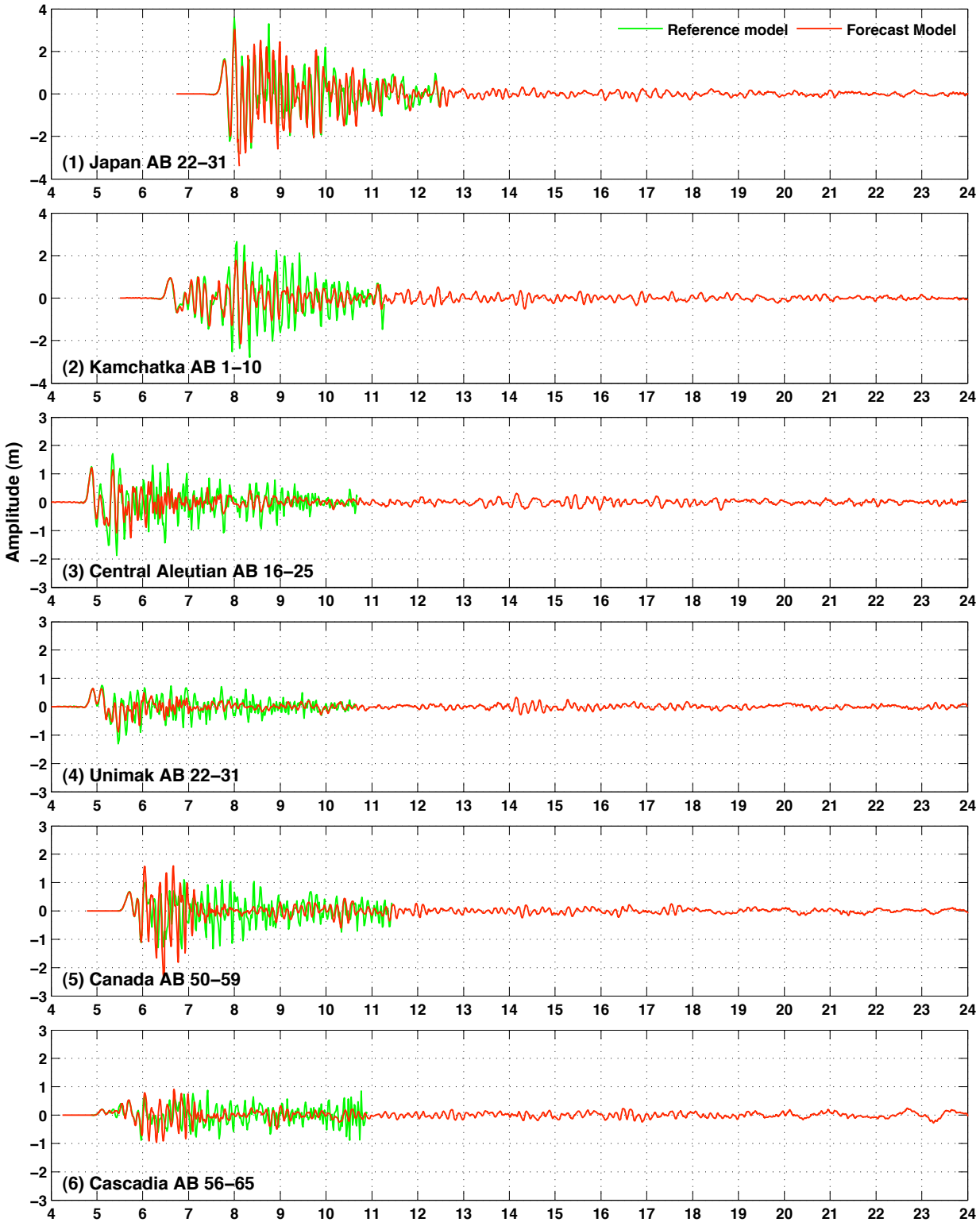

Figure 12: Modeled time series of wave amplitudes at Keauhou warning point for the eighteen simulated magnitude 9.3 tsunamis.

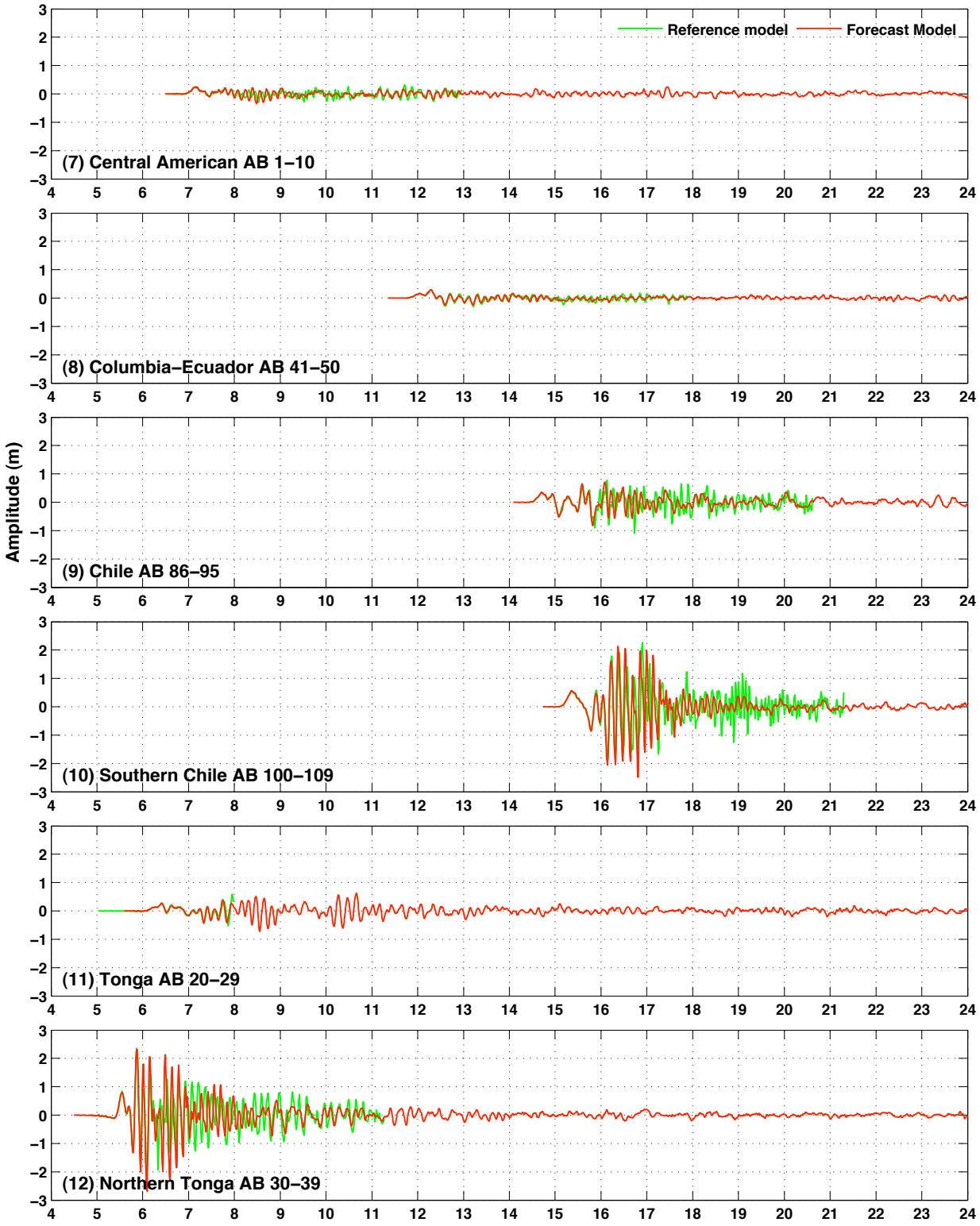

Figure 12: (Continued).

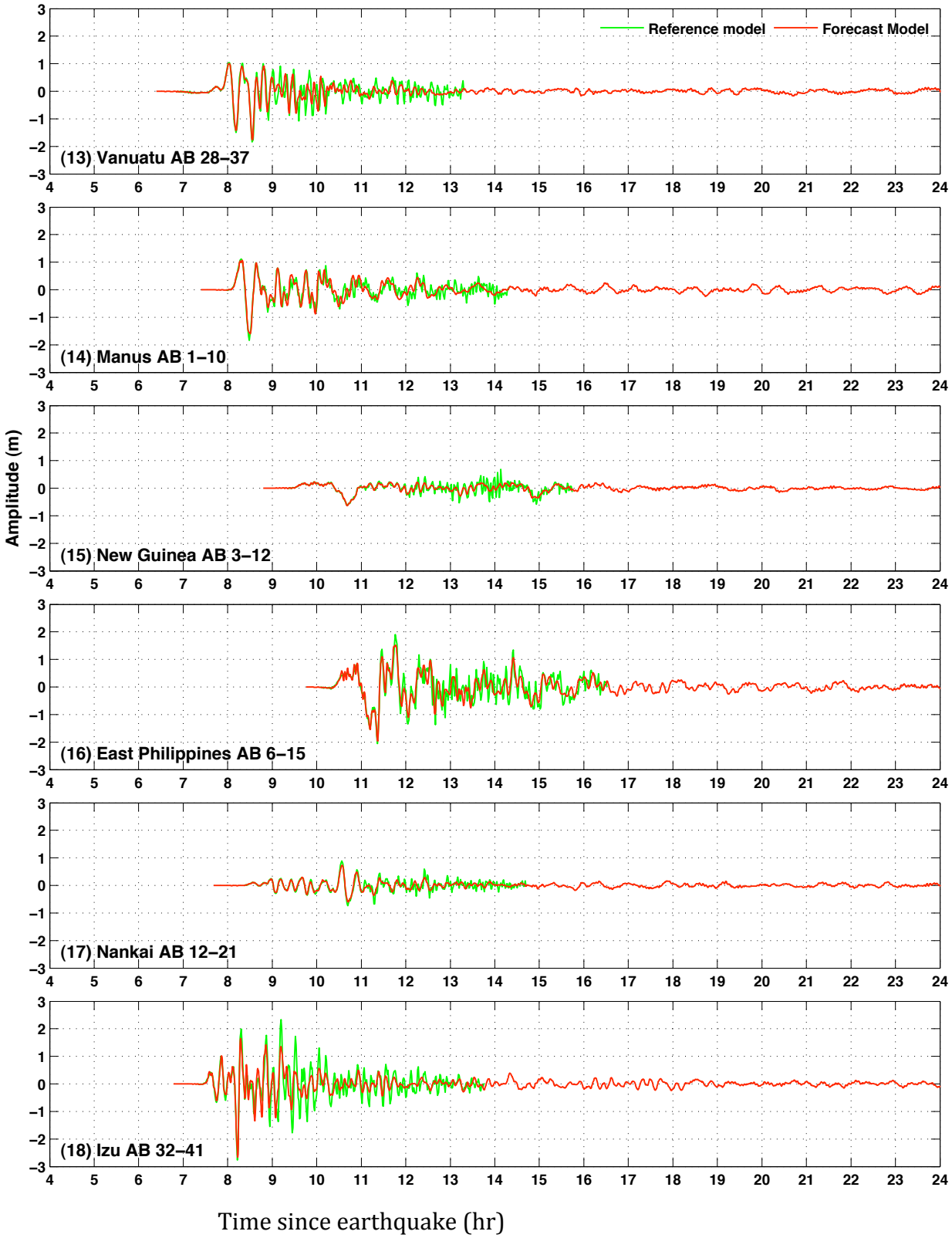

Figure 12: (Continued).

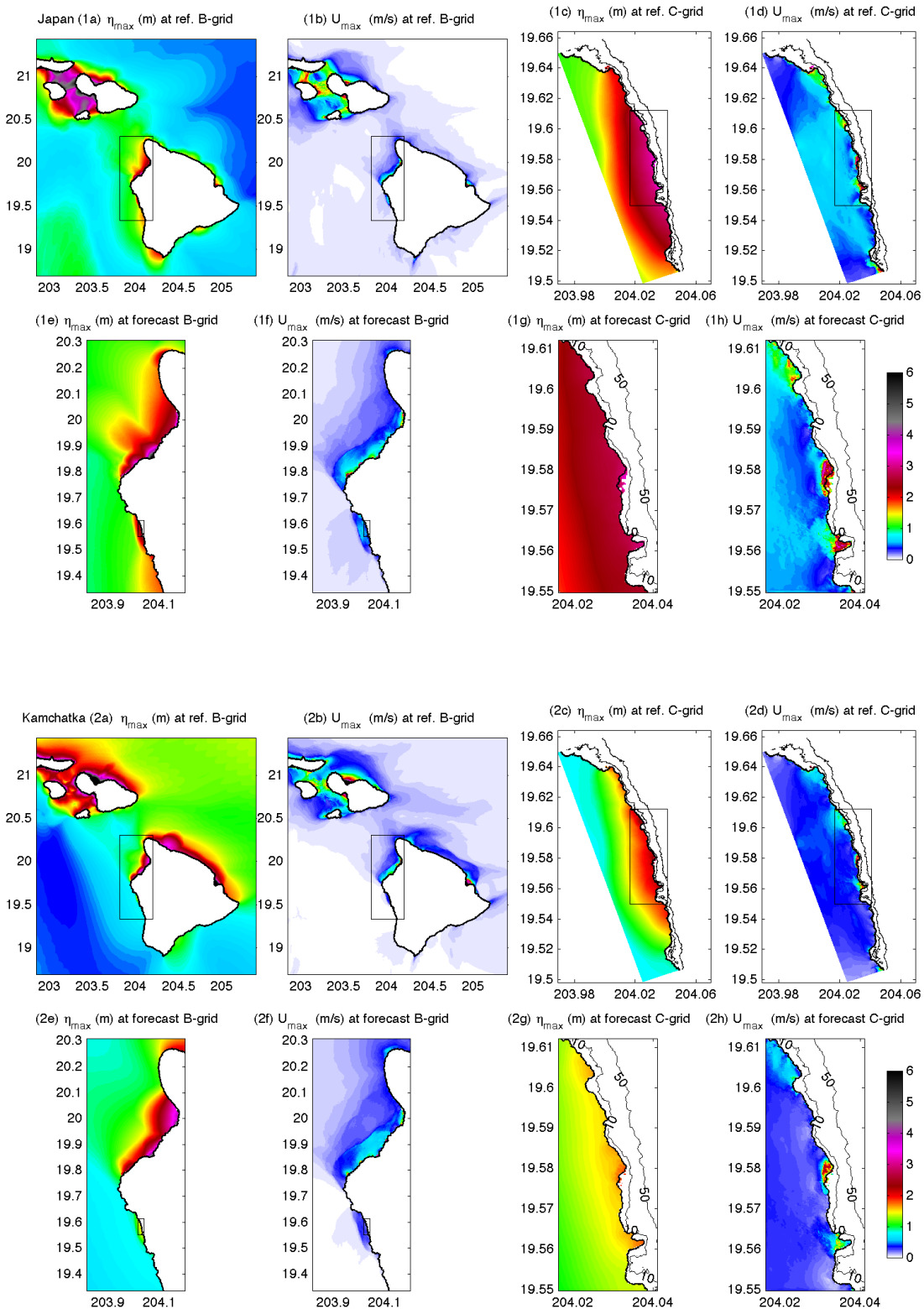

Figure 13: (1-2) Computed maximum sea surface elevation and speed by the Keauhou reference and forecast models for simulated Mw 9.3 (1) Japan and (2) Kamchatka tsunamis.

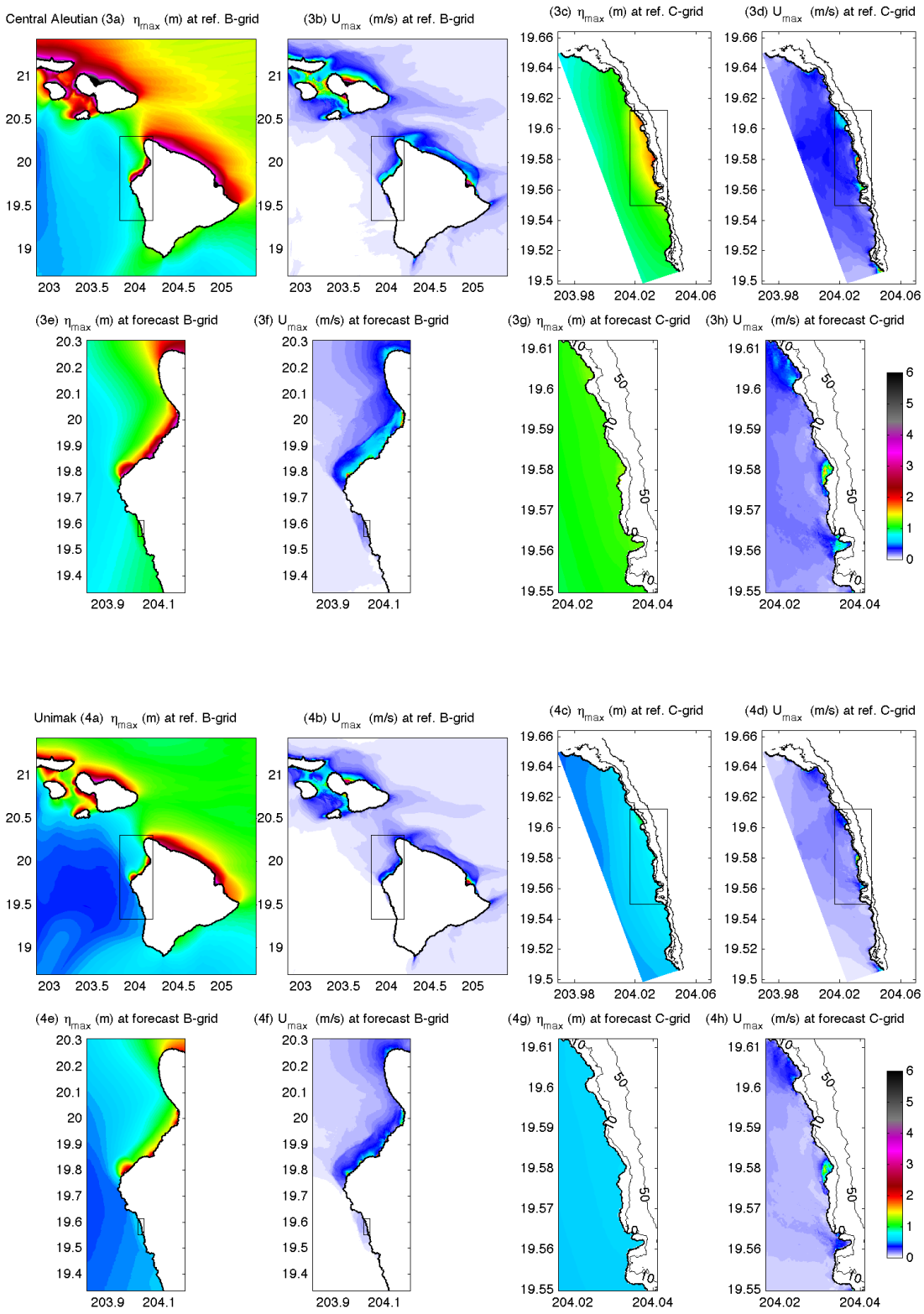

Figure 13 (Continued): (3-4) Computed maximum sea surface elevation and speed by the Keauhou reference and forecast models for simulated Mw 9.3 (3) Central Aleutian and (4) Unimak tsunamis.

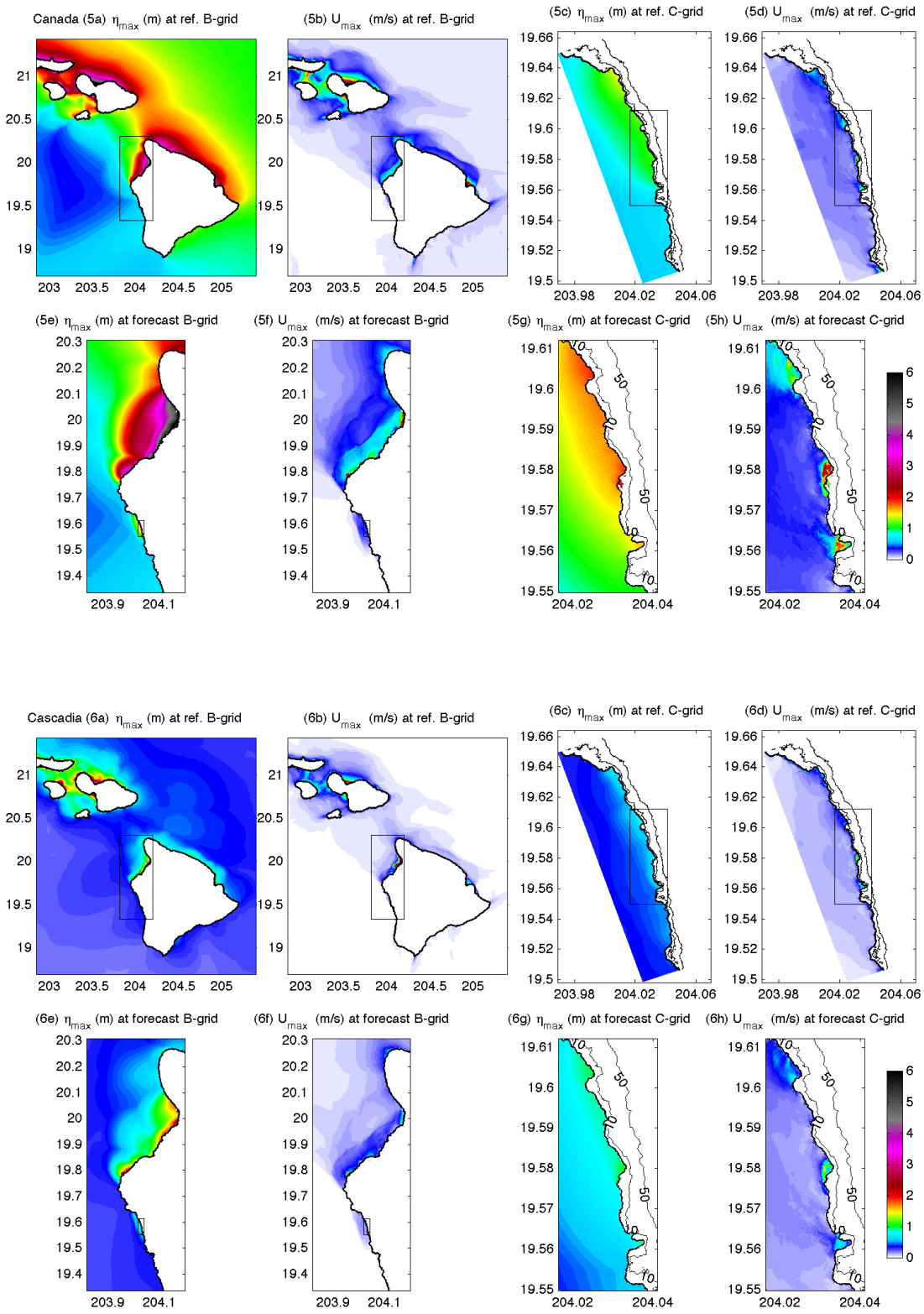

Figure 13 (Continued): (5-6) Computed maximum sea surface elevation and speed by the Keauhou reference and forecast models for simulated Mw 9.3 (5) Canada and (6) Cascadia tsunamis.

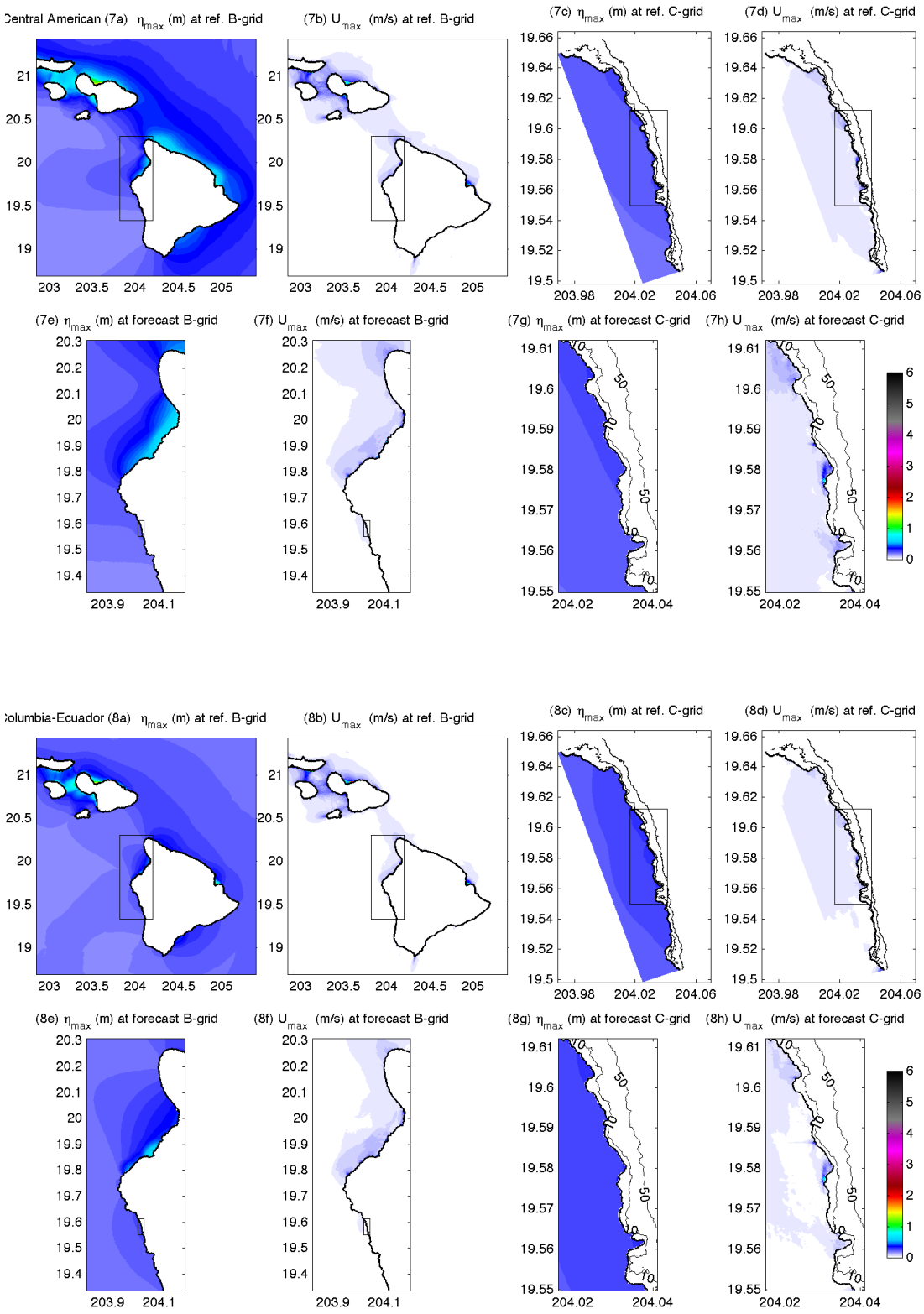

Figure 13 (Continued): (7-8) Computed maximum sea surface elevation and speed by the Keauhou reference and forecast models for simulated Mw 9.3 (7) Central American and (8) Columbia-Ecuador tsunamis.

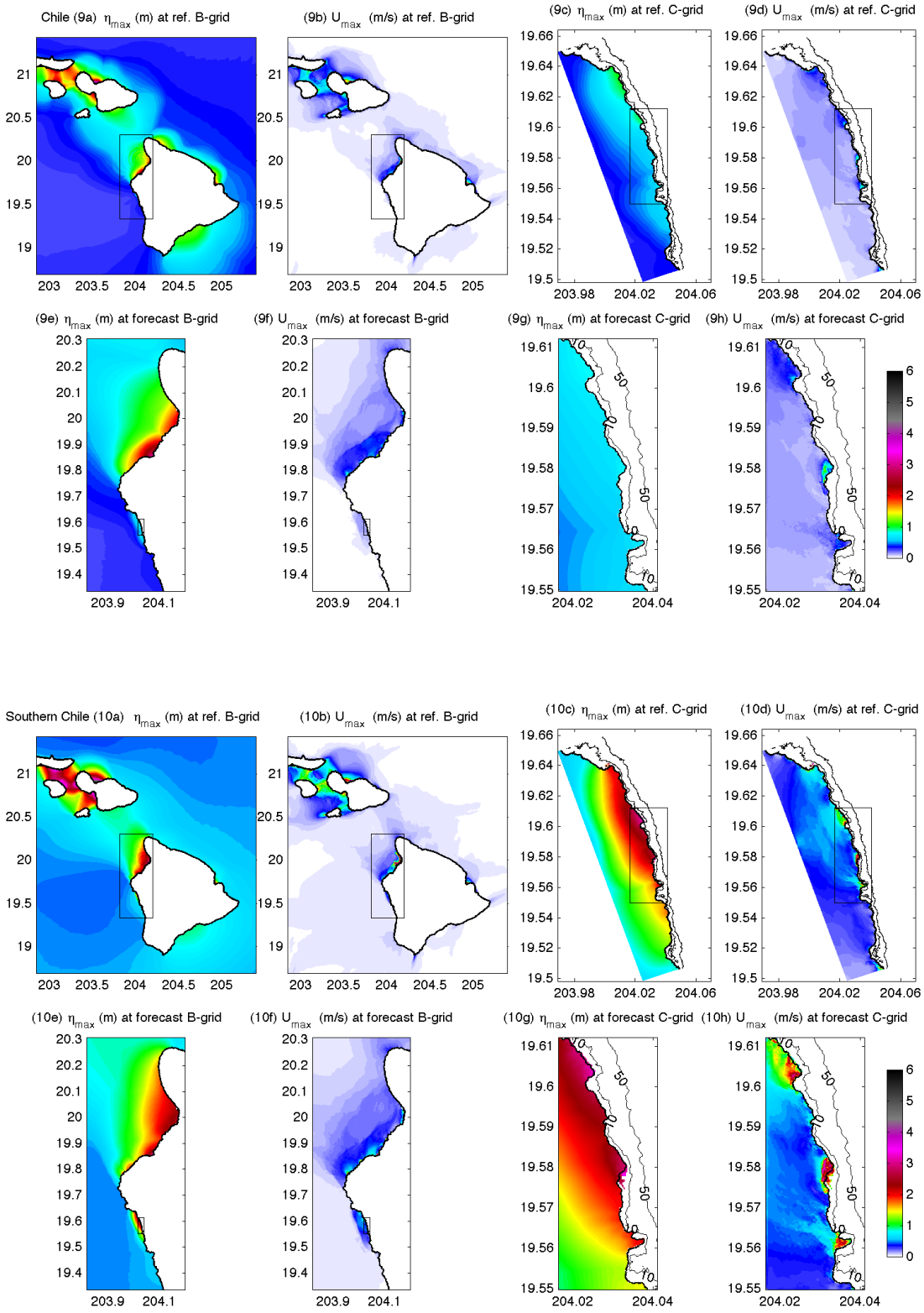

Figure 13 (Continued): (9-10) Computed maximum sea surface elevation and speed by the Keauhou reference and forecast models for simulated Mw 9.3 (9) Chile and (10) Southern Chile tsunamis.

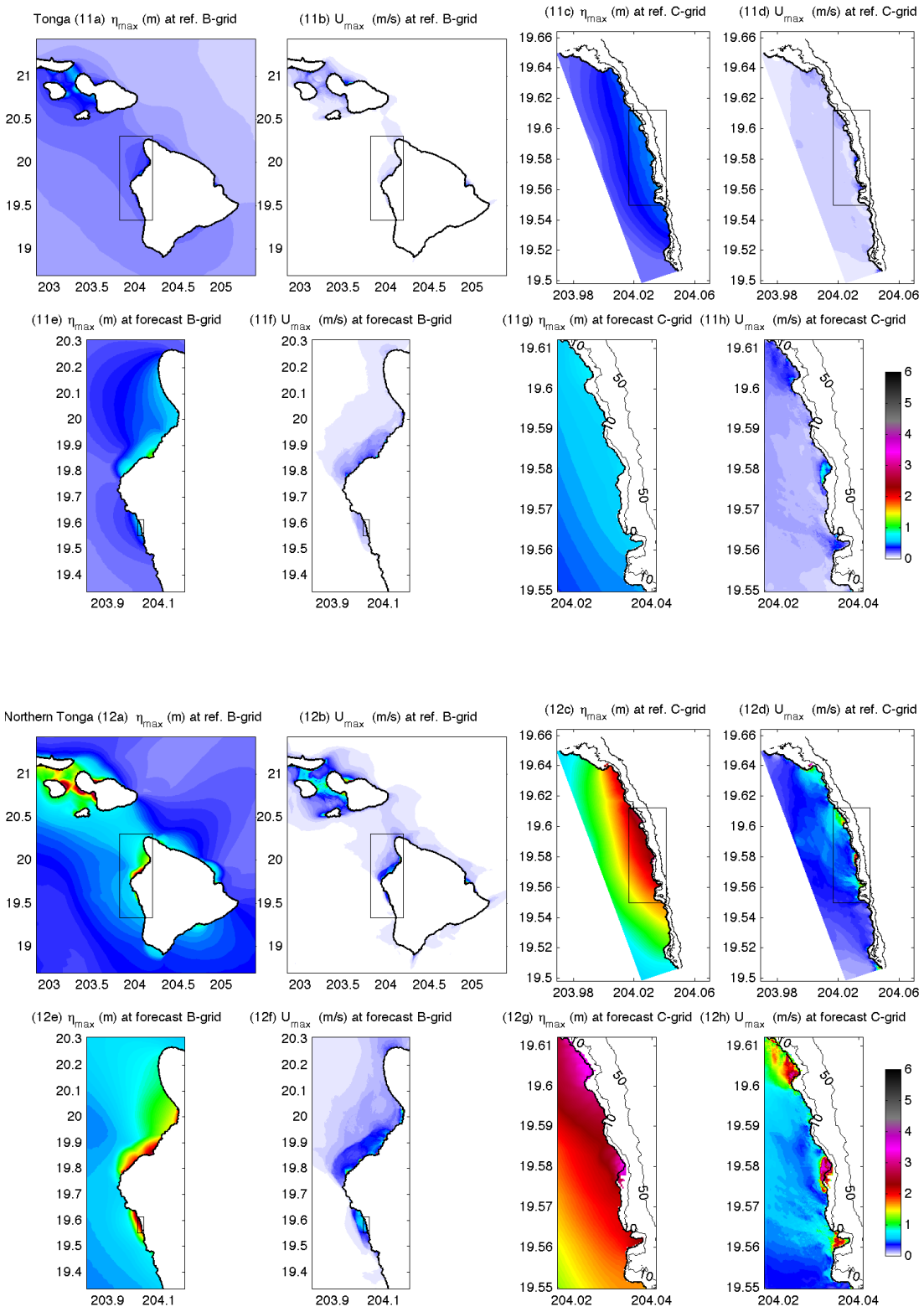

Figure 13 (Continued): (11-12) Computed maximum sea surface elevation and speed by the Keauhou reference and forecast models for simulated Mw 9.3 (11) Tonga and (12) Northern Tonga tsunamis.

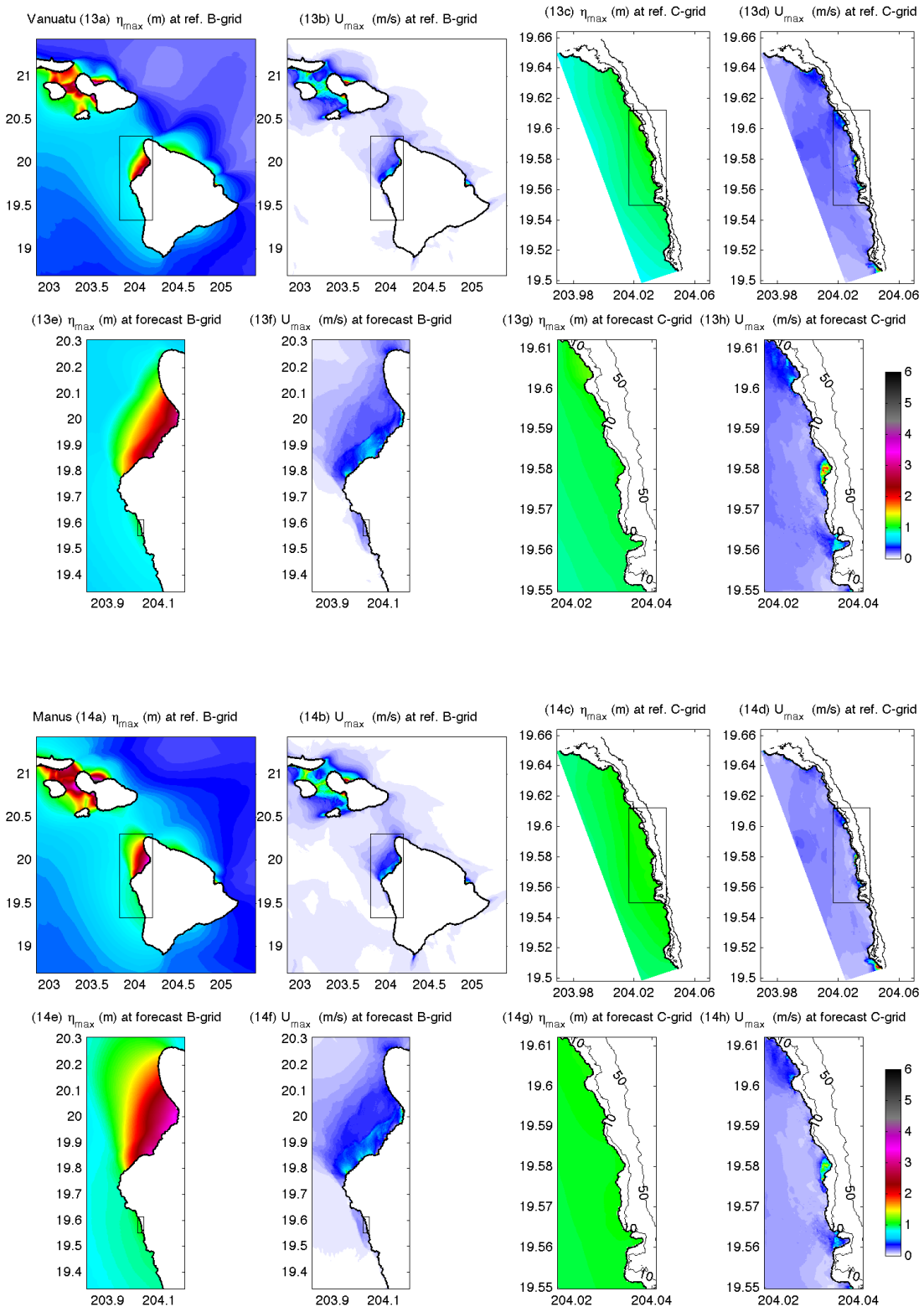

Figure 13 (Continued): (13-14) Computed maximum sea surface elevation and speed by the Keauhou reference and forecast models for simulated Mw 9.3 (13) Vanuatu and (14) Manus tsunamis.

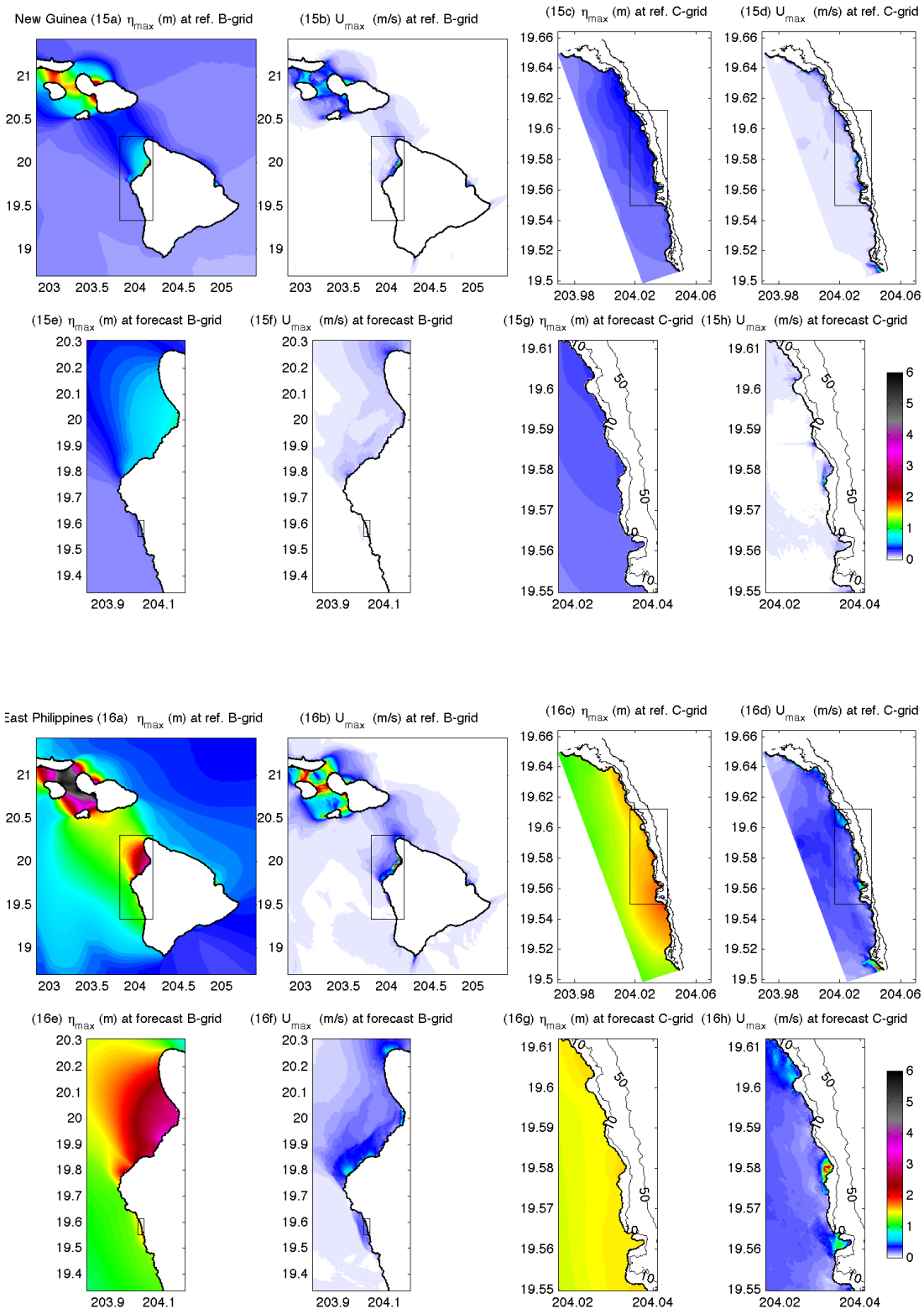

Figure 13 (Continued): (15-16) Computed maximum sea surface elevation and speed by the Keauhou reference and forecast models for simulated Mw 9.3 (15) New Guinea and (16) East Philippines tsunamis.

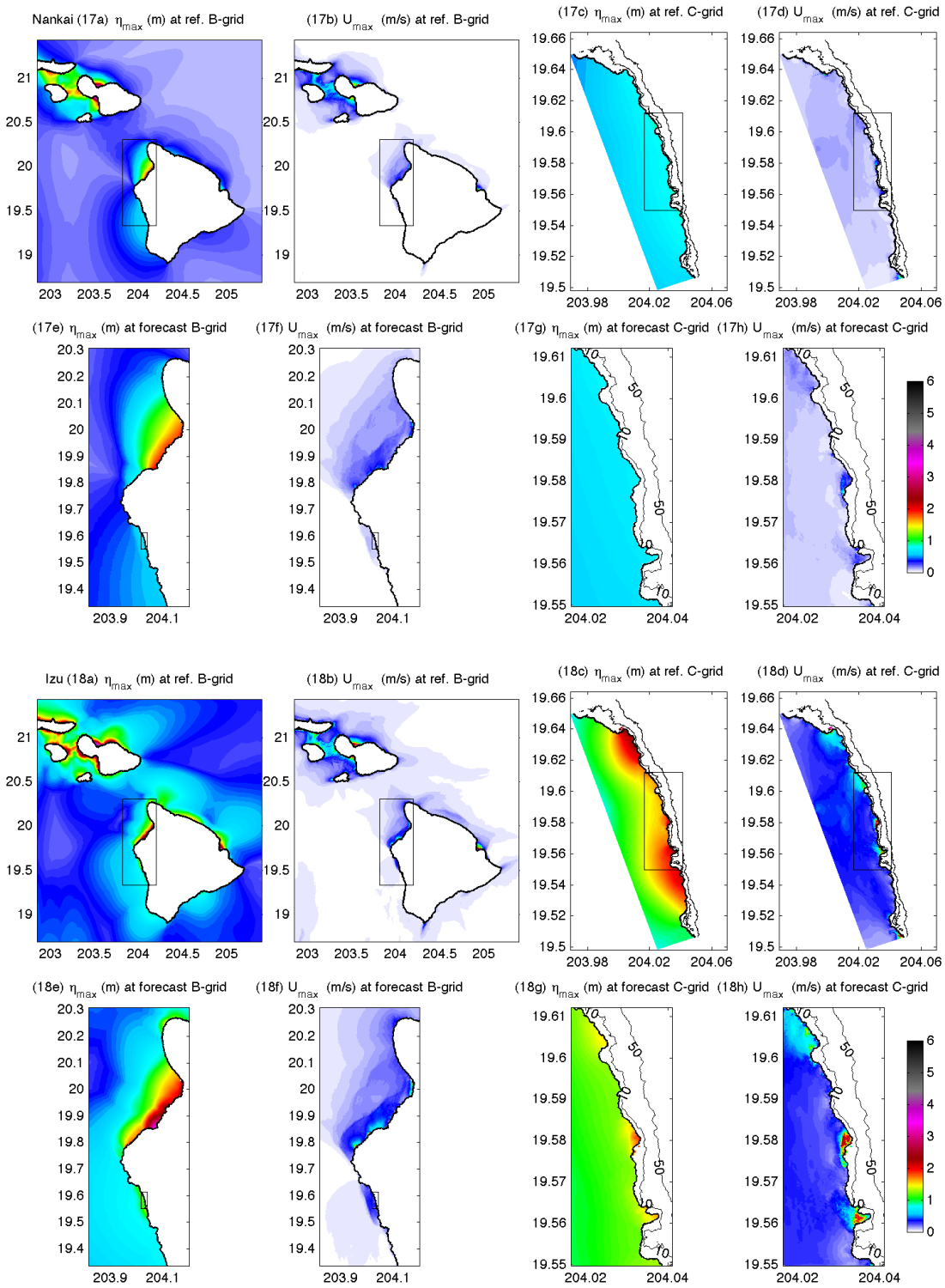

Figure 13 (Continued): (17-18) Computed maximum sea surface elevation and speed by the Keauhou reference and forecast models for simulated Mw 9.3 (17) Nankai and (18) Izu tsunamis.

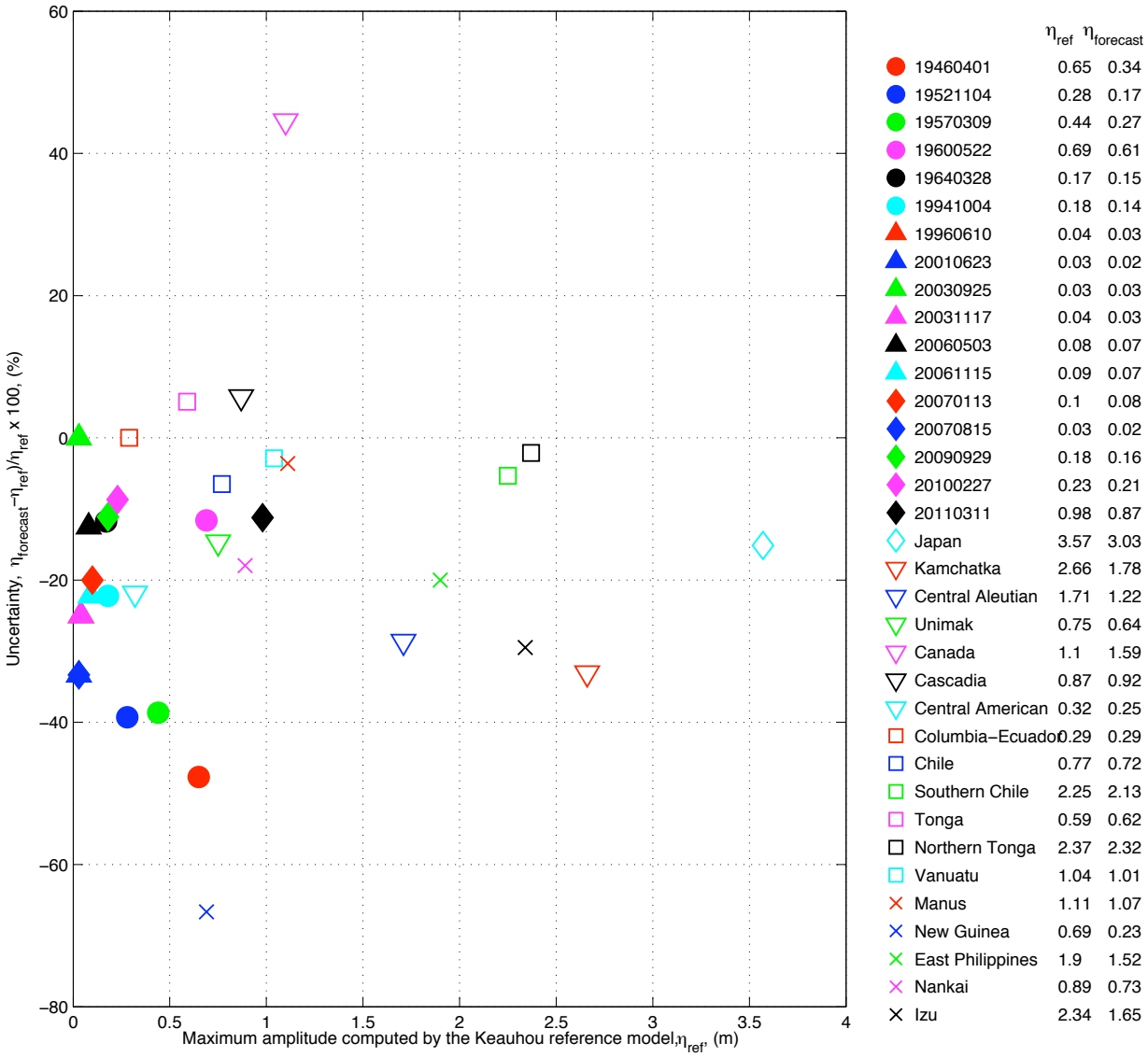

Figure 14: Maximum amplitude at Keauhou Warning point computed by the reference model and forecast model for 35 tsunamis. Filled markers, 17 past tsunamis; open markers, 18 magnitude 9.3 simulated tsunamis.

Appendix C SIFT Testing Report

Keauhou, Hawaii

Jean Newman

1.0 PURPOSE

Forecast models are tested with synthetic tsunami events covering a range of tsunami source locations. Testing is also done with selected historical tsunami events when available.

The purpose of forecast model testing is three-fold. The first objective is to assure that the results obtained with NOAA's tsunami forecast system, which has been released to the Tsunami Warning Centers for operational use, are identical to those obtained by the researcher during the development of the forecast model. The second objective is to test the forecast model for consistency, accuracy, time efficiency, and quality of results over a range of possible tsunami locations and magnitudes. The third objective is to identify bugs and issues in need of resolution by the researcher who developed the Forecast Model or by the forecast software development team before the next version release to NOAA's two Tsunami Warning Centers.

Local hardware and software applications, and tools familiar to the researcher(s), are used to run the Method of Splitting Tsunamis (MOST) model during the forecast model development. The test results presented in this report lend confidence that the model performs as developed and produces the same results when initiated within the forecast application in an operational setting as those produced by the researcher during the forecast model development. The test results assure those who rely on the Keauhou tsunami forecast model that consistent results are produced irrespective of system.

2.0 TESTING PROCEDURE

The general procedure for forecast model testing is to run a set of synthetic tsunami scenarios and a selected set of historical tsunami events through the forecast system application and compare the results with those obtained by the researcher during the forecast model development and presented in the Tsunami Forecast Model Report. Specific steps taken to test the model include:

1. Identification of testing scenarios, including the standard set of synthetic events, appropriate historical events, and customized synthetic scenarios that may have been used by the researcher(s) in developing the forecast model.
2. Creation of new events to represent customized synthetic scenarios used by the researcher(s) in developing the forecast model, if any.
3. Submission of test model runs with the forecast system, and export of the results from A, B, and C grids, along with time series.
4. Recording applicable metadata, including the specific version of the forecast system used for testing.
5. Examination of forecast model results from the forecast system for instabilities in both time series and plot results.
6. Comparison of forecast model results obtained through the forecast system with those obtained during the forecast model development.
7. Summarization of results with specific mention of quality, consistency, and time efficiency.
8. Reporting of issues identified to modeler and forecast software development team.

9. Retesting the forecast models in the forecast system when reported issues have been addressed or explained.

Synthetic model runs were tested on a DELL PowerEdge R510 computer equipped with two Xeon E5670 processors at 2.93 Ghz, each with 12 MBytes of cache and 32GB memory. The processors are hex core and support hyperthreading, resulting in the computer performing as a 24 processor core machine. Additionally, the testing computer supports 10 Gigabit Ethernet for fast network connections. This computer configuration is similar or the same as the configurations of the computers installed at the Tsunami Warning Centers so the compute times should only vary slightly.

Results

The Keauhou forecast model was tested with NOAA's tsunami forecast system version 3.2. The propagation databased used during development was dated in 2011.

The Keauhou, Hawaii forecast model was tested with four synthetic scenarios and one historical tsunami event. Test results from the forecast system and comparisons with the results obtained during the forecast model development are shown numerically in Table C1 and graphically in Figures C1 to C5. The results show that the forecast model is stable and robust, with consistent and high quality results across geographically distributed tsunami sources and mega-event tsunami magnitudes. The model run time (wall clock time) was under 21 minutes for 5 hours of simulation time, and under 17 minutes for 4 hours. This run time is above the 10 minute run time for 4 hours of simulation time that satisfies time efficiency requirements.

Four synthetic events were run on the Keauhou forecast model. The modeled scenarios were stable for all cases tested, with no instabilities or ringing. Results show that the largest modeled height was 300.7 cm and originated in the Kamchatka-Yap-Mariana-Izu-Bonin (KISZ 22-31) source. Amplitudes greater than 100 cm were recorded for 2 out of 4 test sources. The smallest signal of 71.5 cm was recorded at the Central and South America (CSSZ 86-95) source. Direct comparisons, of output from the forecast tool with results of both the historical event (Tohoku 2011) and available development synthetic events, demonstrated that the wave pattern were similar in shape, pattern and amplitude.

Table C1. Table of maximum and minimum amplitudes (cm) at the Keauhou, Hawaii warning point for synthetic and historical events tested using SIFT 3.2 and obtained during development.

Scenario Name	Source Zone	Tsunami Source	α [m]	SIFT Max (cm)	Development Max (cm)	SIFT Min (cm)	Development Min (cm)
Mega-tsunami Scenarios							
KISZ 22-31	Kamchatka-Yap-Mariana-Izu-Bonin	A22-A31, B22-B31	29	300.7	303	-346.6	n/a
ASCZ 56-65	Aleutian-Alaska-Cascadia	A56-A65, B56-B65	29	91.7	92	-96.2	n/a
CSSZ 86-95	Central and South America	A86-A95, B86-B95	29	71.5	72	-81.3	n/a
NTSZ 30-39	New Zealand-Kermadec-Tonga	A30-A39, B30-B39	29	233.9	232	-270.3	n/a
Historical Events							
Tohoku 2011	Kamchatka-Yap-Mariana-Izu-Bonin	4.66 b24 + 12.23 b25+26.31 a26+21.27 b26+22.75 a27 +4.98 b27		87.0	87	-101.4	-101

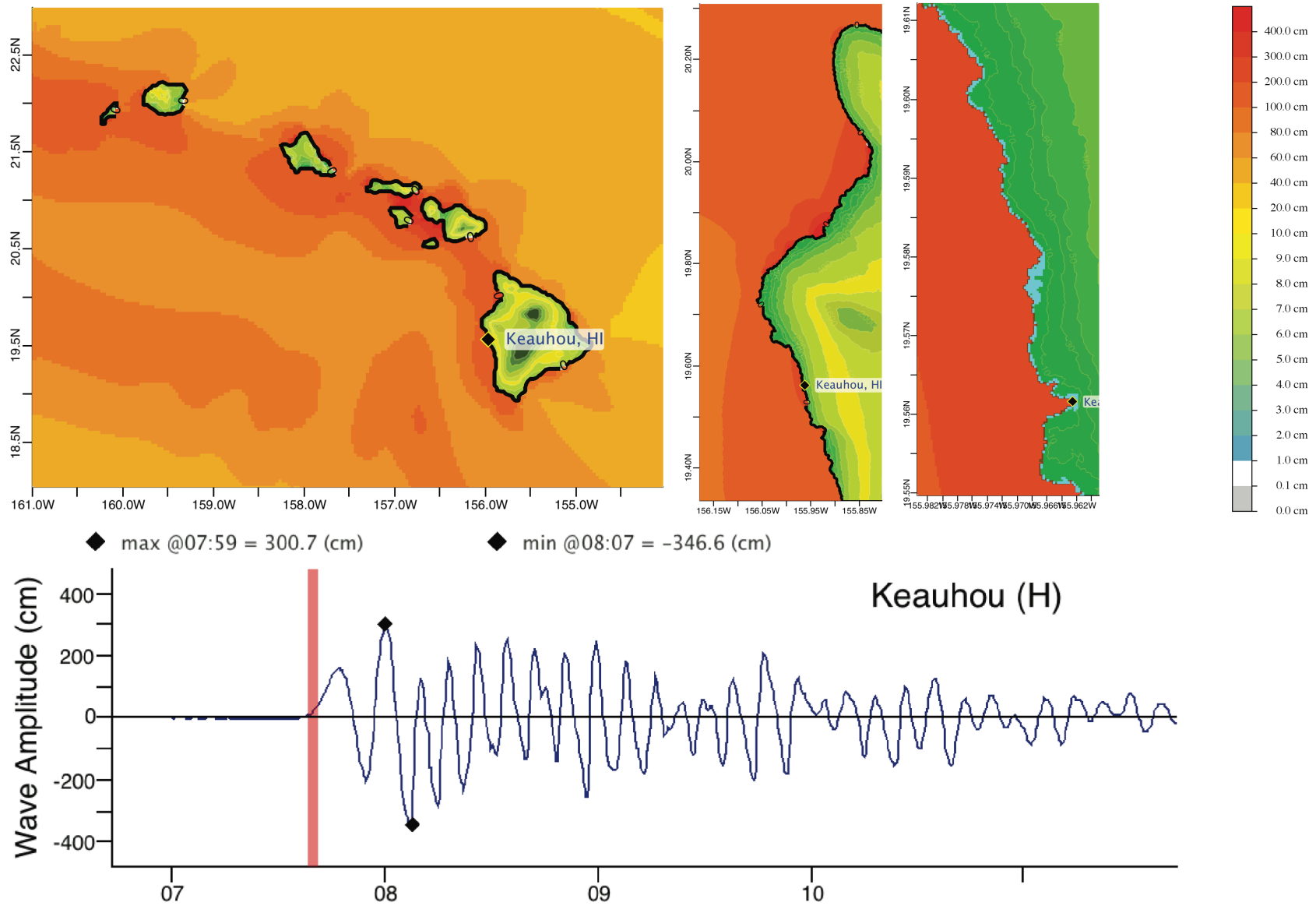

Figure C1: Response of the Keauhou forecast model to synthetic scenario KISZ 22-31 (alpha=29). Maximum sea surface elevation for (a) A-grid, b) B-grid, c) C-grid. Sea surface elevation time series at the C-grid warning point (d).

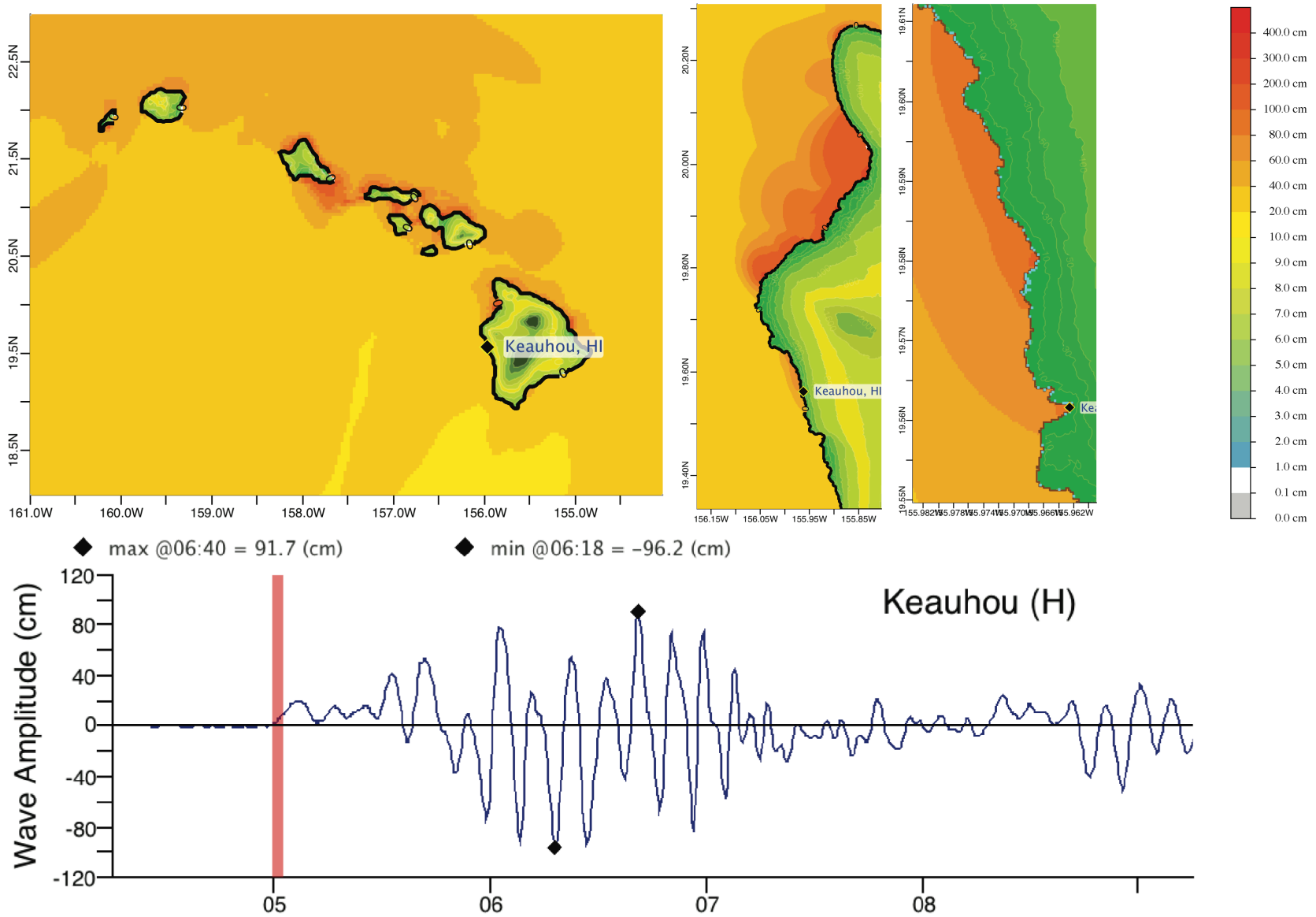

Figure C2: Response of the Keauhou forecast model to synthetic scenario ACSZ 56-65 (alpha=29). Maximum sea surface elevation for (a) A-grid, b) B-grid, c) C-grid. Sea surface elevation time series at the C-grid warning point (d).

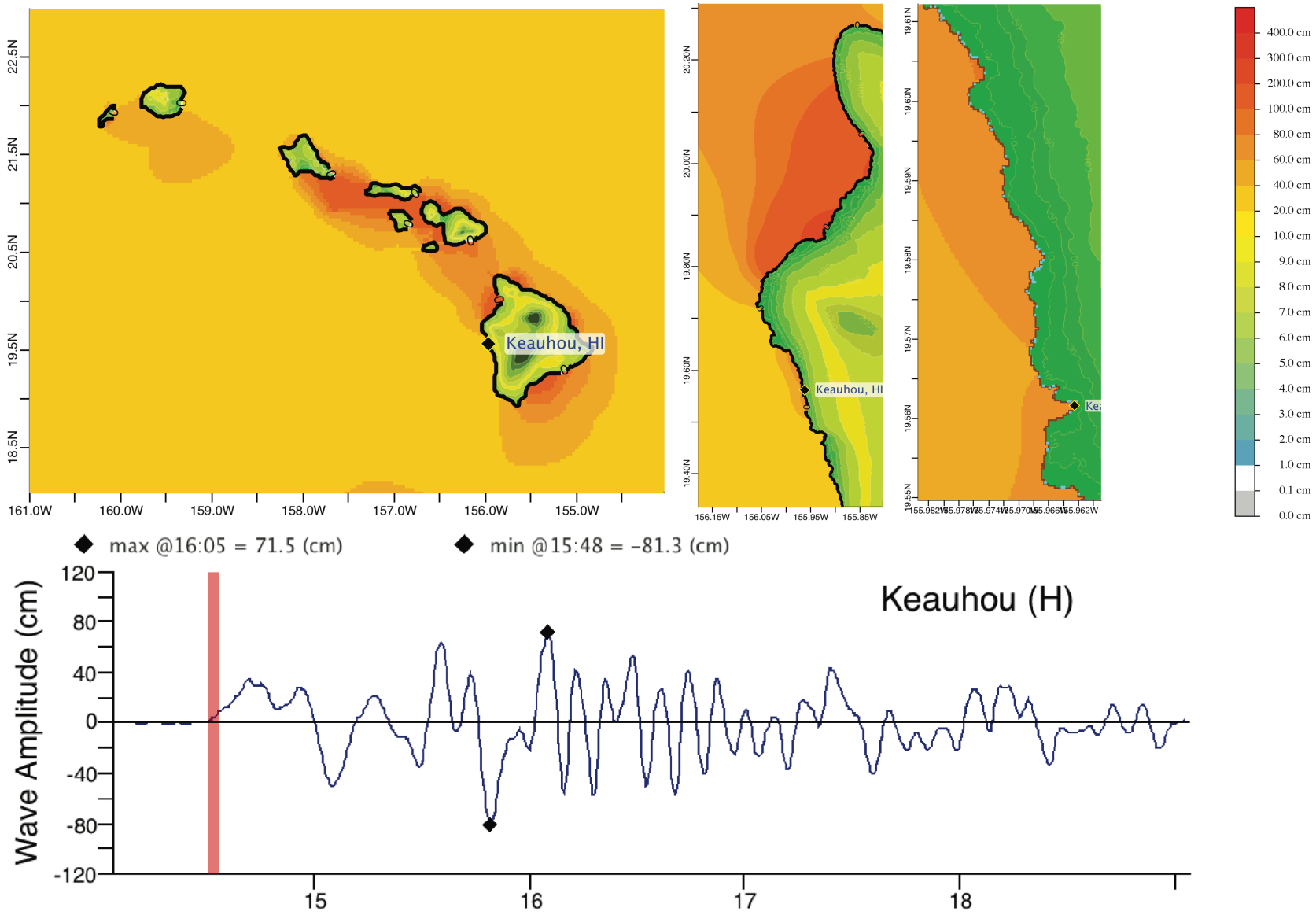

Figure C3: Response of the Keauhou forecast model to synthetic scenario CSSZ 86-95 (alpha=29). Maximum sea surface elevation for (a) A-grid, b) B-grid, c) C-grid. Sea surface elevation time series at the C-grid warning point (d).

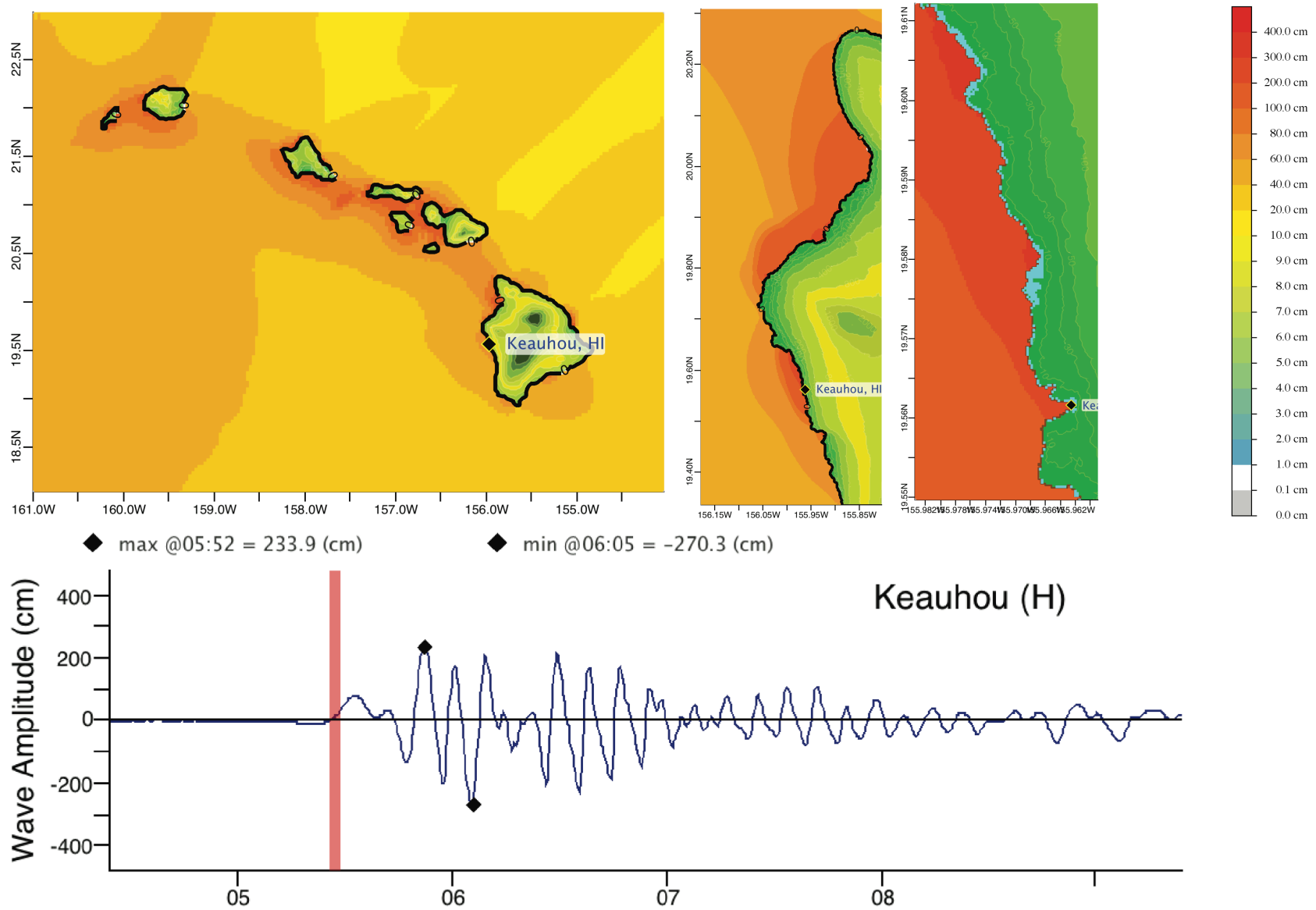

Figure C4: Response of the Keauhou forecast model to synthetic scenario NTSZ 30-39 (alpha=29). Maximum sea surface elevation for (a) A-grid, b) B-grid, c) C-grid. Sea surface elevation time series at the C-grid warning point (d).

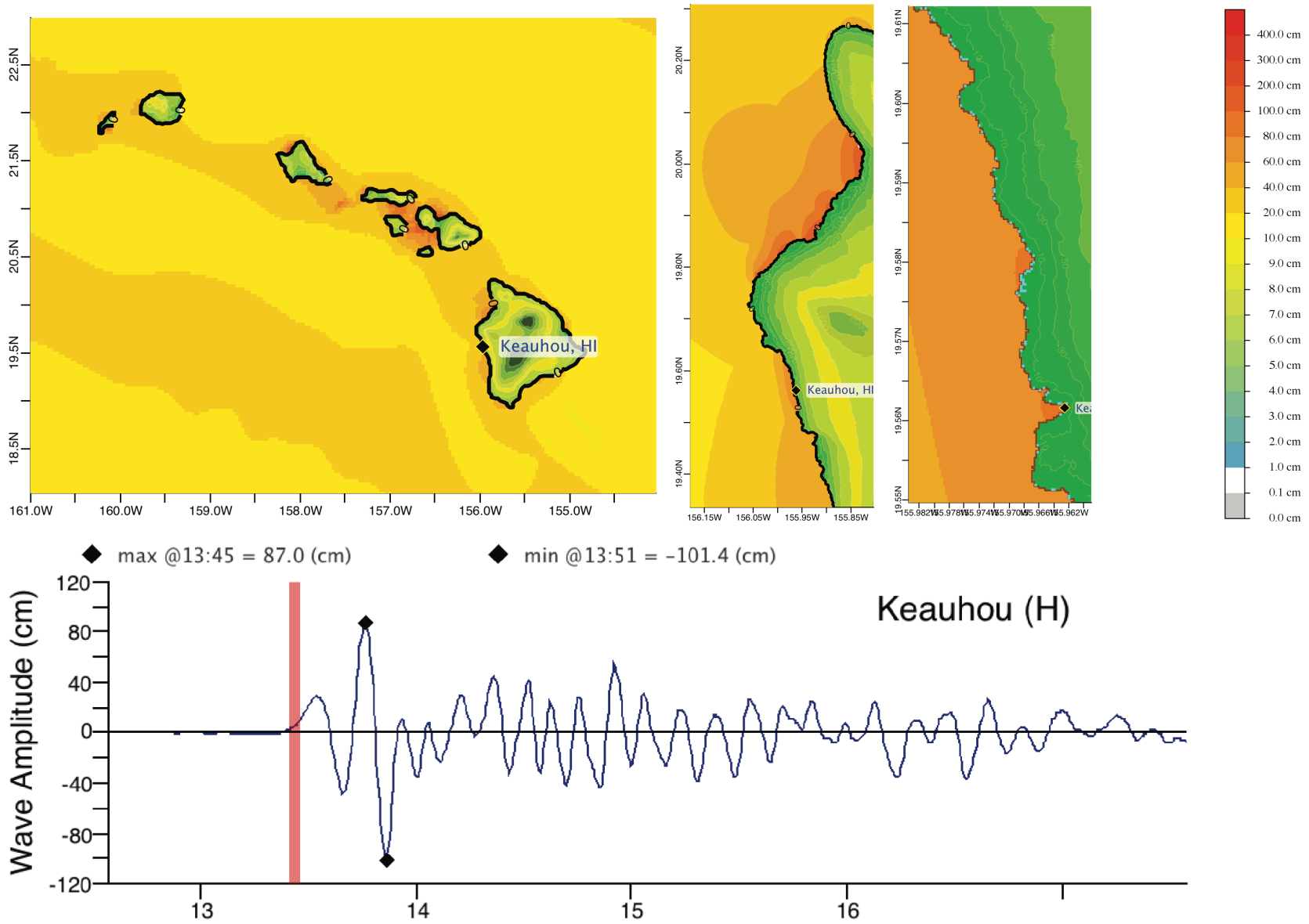

Figure C5: Response of the Keauhou forecast model to the 2011 Tohoku tsunami. Maximum sea surface elevation for (a) A-grid, b) B-grid, c) C-grid. Sea surface elevation time series at the C-grid warning point (d).